

# Parameter space of baryogenesis in the $\nu$ MSM

---

S. Eijima,<sup>a</sup> M. Shaposhnikov,<sup>b</sup> I. Timiryasov<sup>b</sup>

<sup>a</sup>*Intituut-Lorentz, Leiden University, Niels Bohrweg 2, 2333 CA Leiden, The Netherlands*

<sup>b</sup>*Institute of Physics, Laboratory for Particle Physics and Cosmology,  
École Polytechnique Fédérale de Lausanne, CH-1015 Lausanne, Switzerland*

*E-mail:* [Eijima@lorentz.leidenuniv.nl](mailto:Eijima@lorentz.leidenuniv.nl), [Mikhail.Shaposhnikov@epfl.ch](mailto:Mikhail.Shaposhnikov@epfl.ch),  
[Inar.Timiryasov@epfl.ch](mailto:Inar.Timiryasov@epfl.ch)

**ABSTRACT:** The Standard Model accompanied with two right-handed neutrinos with masses below the weak scale can explain the observed baryon asymmetry of the Universe. Moreover, this model is at least partially testable in the forthcoming experiments such as NA62, SHiP, and MATHUSLA. The remarkable progress in understanding of various rates entering the kinetic equations describing the asymmetry generation along with considerable improvements of the numerical procedures allow us to perform a comprehensive analysis of the parameter space of the model. We find that the region of parameters leading to successful baryogenesis is notably larger than it was previously obtained for light HNLs. Our results are presented in a way that they can be readily used for studies of sensitivity of various experiments searching for the right-handed neutrinos responsible for the baryon asymmetry of the Universe. We also present a detailed comparison with the studies by other groups.

---

## Contents

<b>1</b>	<b>Introduction</b>	<b>2</b>
<b>2</b>	<b>The <math>\nu</math>MSM</b>	<b>3</b>
<b>3</b>	<b>Experimentally observable quantities</b>	<b>5</b>
3.1	The total mixing	5
3.2	Individual mixings	6
<b>4</b>	<b>Cosmologically motivated values of mixings</b>	<b>7</b>
<b>5</b>	<b>Open access datasets</b>	<b>8</b>
<b>6</b>	<b>Generation of the baryon asymmetry</b>	<b>9</b>
6.1	Kinetic equations	9
6.2	Gradual freeze-out of sphalerons	14
6.3	Physics of asymmetry generation	15
<b>7</b>	<b>Numerical analysis of the kinetic equations</b>	<b>16</b>
7.1	The procedure for numerical solution of the equations	16
7.2	Analysis of the equations	17
<b>8</b>	<b>Study of the parameter space</b>	<b>20</b>
8.1	Total mixing	20
8.2	Individual mixings	21
<b>9</b>	<b>Comparison with other works</b>	<b>21</b>
<b>10</b>	<b>Conclusions and outlook</b>	<b>26</b>
<b>A</b>	<b>Mixings of HNLs and active neutrinos</b>	<b>27</b>
<b>B</b>	<b>Derivation of the kinetic equations in Higgs phase</b>	<b>29</b>
B.1	Overview of the procedure	29
B.2	Lagrangian and Hamiltonian	30
B.3	Commutators and averaging	33
B.4	The final form of the equations	36
<b>C</b>	<b>Rates in the symmetric phase</b>	<b>37</b>
<b>D</b>	<b>Benchmark points</b>	<b>37</b>

---

# 1 Introduction

Neutrino oscillations are among the three experimentally established phenomena beyond the Standard Model (SM). Two others are the baryon asymmetry of the Universe (BAU) and elusive Dark Matter (DM).

Flavour oscillations of active neutrinos are prohibited within the canonical SM because of conservation of individual global lepton numbers. The simplest and, probably, the most natural way of describing neutrino masses is introduction of right-handed neutrinos into the model [1–6]. The oscillation data is compatible with the presence of two or more right-handed neutrinos. In contrast to the SM particles, there are no symmetries prohibiting Majorana mass terms for right-handed neutrinos. The scale of this mass term is not fixed by neutrino oscillations and can vary by many orders of magnitude.

In refs. [7, 8] it was suggested that the minimal extension of the SM with three right-handed neutrinos with masses *below the electroweak scale*—the  $\nu$ MSM—can simultaneously address the problems of neutrino oscillations, dark matter (DM) and BAU. Two right-handed neutrinos (following the PDG we will also refer to right-handed neutrinos as heavy neutral leptons or HNLs) that are responsible for the production of the BAU in the  $\nu$ MSM may have masses in the GeV range. They could be searched for in current and planned experiments. The lightest right-handed neutrino may play the role of the DM particle [9–12], [7].

Baryogenesis with GeV scale HNLs suggested in ref. [13] and refined in ref. [8] has attracted a lot of attention and a significant progress has been achieved recently. An incomplete list of related works includes [14–40]. The structure of kinetic equations proposed in [8] remained unchanged, however, understanding of the rates entering into these equations has considerably improved [28, 36, 37]. The role of neutrality of electroweak plasma has been clarified [24, 28, 38]. Dynamics of the freeze-out of the baryon number has been carefully studied [38].

The testability of the model has also drawn a considerable attention from the experimental side and the new searches for HNLs were carried out [41–47]. There are several proposals of the experiments which will be very sensitive to the HNLs of the  $\nu$ MSM: NA62 in the beam dump mode [48], SHiP [49] and MATHUSLA [50].<sup>1</sup> Of course, it is important to understand whether the HNLs responsible for baryogenesis can be found in these experiments. There were already several studies of the parameter space of the model [21, 23, 32–34] relevant for the current or near-future experiments.

Still, these investigations are not complete. In the present work we improve the analysis by (i) using the kinetic equations derived in ref. [36]. These equations account for both fermion number conserving and violating reactions, (ii) accounting for the neutrality of the electroweak plasma and the non-instantaneous freeze-out of the baryon number using methods suggested in ref. [38], and (iii) using the fast numerical code that allows scanning over a wider region of the parameter space. We find that the region of parameters leading to the successful baryogenesis with light HNLs is notably larger than it was previously

---

<sup>1</sup>Also the recently proposed CODEX-b [51] and FASER [52, 53] will be probably sensitive to the HNLs of the  $\nu$ MSM. Note that indirect searches, such as  $\mu \rightarrow e\gamma$ , are not sensitive to the  $\nu$ MSM [54].

obtained. The results are presented in a way that they can be used for a detailed study of sensitivity of different experiments.

The paper is organized as follows. First, we introduce the  $\nu$ MSM and the parameters of the model in section 2. Then we describe the experimentally relevant quantities in section 3 and present the cosmologically favourable values of these quantities in section 4. These values are determined by imposing the requirement of the successful baryogenesis. In section 5 we provide all necessary information on the open-access datasets. All theoretical and technical details are presented in the subsequent sections. In section 6 we overview the kinetic equations derived in ref. [36]. We discuss our approach for the numerical solution of these equations and describe the impact of the improvements in section 7. The study of the parameter space is performed in section 8. Section 9 contains a detailed comparison with the works [21, 23, 32–34, 37, 40]. We summarise in section 10. Appendix A describes the mixings of active neutrinos and HNLs in our parametrization of Yukawas. Appendix B contains the derivation of the kinetic equations. Finally, in appendix D we list several sets of the model parameters along with the corresponding values of the BAU. These sets can be used by other groups as benchmarks to compare numerical results.

## 2 The $\nu$ MSM

In this section we fix our notations by introducing the Lagrangian of the  $\nu$ MSM [7, 8] and the parametrization of Yukawa couplings [55, 56]. Even though these expressions are well known and have been presented many times, we list them to make the paper self-consistent.

The Lagrangian of the  $\nu$ MSM is the usual see-saw one [1–6]

$$\mathcal{L} = \mathcal{L}_{SM} + i\bar{\nu}_{R_I}\gamma^\mu\partial_\mu\nu_{R_I} - F_{\alpha I}\bar{L}_\alpha\tilde{\Phi}\nu_{R_I} - \frac{M_{IJ}}{2}\bar{\nu}_{R_I}^c\nu_{R_J} + h.c., \quad (2.1)$$

where  $\mathcal{L}_{SM}$  is the Lagrangian of the SM,  $\nu_{R_I}$  are right-handed neutrinos labelled with the generation indices  $I, J = 1, 2, 3$ ,  $F_{\alpha I}$  is the matrix of Yukawa couplings,  $L_\alpha$  are the left-handed lepton doublets labelled with the flavour index  $\alpha = e, \mu, \tau$  and  $\tilde{\Phi} = i\sigma_2\Phi^*$ ,  $\Phi$  is the Higgs doublet. We work in a basis where charged lepton Yukawa couplings and the Majorana mass term for the right-handed neutrinos  $M_{IJ}$  are diagonal.

In the broken phase, the Higgs field acquires a temperature dependent vacuum expectation value  $\langle\Phi(T)\rangle$ , which is 174.1 GeV at zero temperature. The Yukawa couplings in the Lagrangian (2.1) lead to the Dirac mass terms  $[M_D]_{\alpha I} = F_{\alpha I}\langle\Phi\rangle$ . The  $6 \times 6$  symmetric mass matrix of neutrinos can be diagonalized by a complex orthogonal transformation. We will restrict ourselves to the see-saw limit  $|[M_D]_{\alpha I}| \ll M_I$ . In this limit the active neutrino flavour states are given by

$$\nu_{L_\alpha} = U_{\alpha i}^{PMNS}\nu_i + \Theta_{\alpha I}N_I^c, \quad (2.2)$$

where  $U^{PMNS}$  is the Pontecorvo-Maki-Nakagawa-Sakata (PMNS) matrix [57, 58],  $\nu_i$  are mass eigenstates of active neutrinos,  $N_I$  are the mass eigenstate of HNLs. The active-sterile mixing matrix in the leading order of the see-saw mechanism is

$$\Theta_{\alpha I} = \frac{\langle\Phi\rangle F_{\alpha I}}{M_I}. \quad (2.3)$$

The parameters of the theory (2.1) are restricted by the see-saw mechanism since one has to reproduce the observed values of the mass differences and mixing angles for the active neutrinos [59].<sup>2</sup> A convenient parametrization of the Yukawa couplings which automatically accounts for these observables was proposed by Casas and Ibarra in ref. [55]. The application of the Casas-Ibarra parametrization to the  $\nu$ MSM has been studied in ref. [56]. In the matrix form, the Yukawa couplings entering the Lagrangian (2.1) read (in the notations of refs. [36, 38])

$$F = \frac{i}{\langle \Phi(0) \rangle} U^{PMNS} m_\nu^{1/2} \Omega m_N^{1/2}, \quad (2.4)$$

where  $m_\nu$  and  $m_N$  are the diagonal mass matrices of the three active neutrinos and HNLs correspondingly. The matrix  $\Omega$  is an arbitrary complex orthogonal  $\mathcal{N}_\nu \times \mathcal{N}_N$  matrix, where  $\mathcal{N}_\nu$  is the number of left-handed neutrinos and  $\mathcal{N}_N$  is the number of right-handed neutrinos.

In the  $\nu$ MSM, the lightest HNL  $N_1$  is the dark matter particle. A combination of Lyman- $\alpha$  and X-ray constraints puts strong bounds on the magnitude of its Yukawa couplings, see [60] and references therein. As a result,  $N_1$  is almost decoupled and does not contribute to the see-saw masses of active neutrinos. Therefore, the masses and mixings of active neutrinos correspond to the case of two HNLs. In this case the matrix  $\Omega$  can be chosen in the form

$$\Omega = \begin{pmatrix} 0 & 0 \\ \cos \omega & \sin \omega \\ -\xi \sin \omega & \xi \cos \omega \end{pmatrix} \quad \text{for NH}, \quad (2.5)$$

$$\Omega = \begin{pmatrix} \cos \omega & \sin \omega \\ -\xi \sin \omega & \xi \cos \omega \\ 0 & 0 \end{pmatrix} \quad \text{for IH}, \quad (2.6)$$

with a complex mixing angle  $\omega$ . The sign parameter is  $\xi = \pm 1$ . We fix it to be  $\xi = +1$ , since the change of the sign of  $\xi$  can be compensated by  $\omega \rightarrow -\omega$  along with  $N_3 \rightarrow -N_3$  [61]. Throughout this work, we will use the abbreviations NH and IH to refer to the normal and inverted hierarchy of neutrino masses. In what follows it is convenient to introduce

$$X_\omega = \exp(\text{Im } \omega). \quad (2.7)$$

In the case of two right-handed neutrinos, the PMNS matrix contains only two  $CP$ -violating phases, one Dirac  $\delta$  and one Majorana  $\eta$ , see Appendix A for the details of our parametrization of the PMNS matrix. Two Majorana masses in (2.1) can be parametrized by the common mass  $M$  and the Majorana mass difference  $\Delta M$ . Note that the *physical* mass difference controlling the oscillations of two HNLs is a sum of  $\Delta M$  and a term proportional to the product of Yukawa couplings with  $\langle \Phi \rangle$ . The expression for this mass difference can be found in ref. [15].

---

<sup>2</sup>The NuFIT group has recently released an updated global analysis of neutrino oscillation measurements, *NuFIT 3.2 (2018)*, [www.nu-fit.org](http://www.nu-fit.org). In our analysis, we use these updated data. The most important update of v3.2 is the  $3\sigma$  bound on the value of the Dirac phase  $\delta$ . In the inverted hierarchy case  $\delta$  is no longer compatible with zero. We will comment on this in section 8.

We end up with six free parameters of the theory which are listed in table 1 along with their ranges considered in this work. The common mass  $M$  of HNLs is restricted to the

$M$ , GeV	$\log_{10}(\Delta M/\text{GeV})$	$\text{Im } \omega$	$\text{Re } \omega$	$\delta$	$\eta$
$[0.1 - 10]$	$[-17, -1]$	$[-7, 7]$	$[0, 2\pi]$	$[0, 2\pi]$	$[0, 2\pi]$

**Table 1.** Parameters of the theory: common mass; mass difference;  $\text{Im } \omega$ ;  $\text{Re } \omega$ ; Dirac and Majorana phases. In the second line we indicate the ranges of these parameters which were considered in this work.

$[0.1 - 10]$  GeV interval. The smaller masses are in tension with the Big Bang nucleosynthesis (BBN) [62]. Heavier HNLs, which we do not consider in this work, deserve a separate study. The ranges of the Majorana mass difference  $\Delta M$  and  $\text{Im } \omega$  are determined by the a posteriori requirement of generating enough BAU. The real part of the complex angle  $\omega$  plays a role of a phase, therefore it is enough to restrict it, along with the single Majorana phase, to the interval  $[0, 2\pi]$ . The range of the Dirac phase  $\delta$  is somewhat more subtle since it was restricted in the recent global analysis of neutrino oscillation measurements. We will comment on this in section 8.

Note that the relation (2.4) is not an isomorphism, i.e. more than one set of the parameters lead to the same Yukawas  $F_{\alpha I}$  and therefore are physically equivalent. Still, the parametrization (2.4) spans all possible values of Yukawas compatible with the oscillation data. Dependence of the resulting BAU on the Yukawas (and parameters in table 1) is in general very complicated. Therefore a thorough study of the parameter space of the model is required in order to determine the boundary of the region where successful baryogenesis is possible in terms of the experimentally interesting quantities.

### 3 Experimentally observable quantities

The parameters listed in table 1 are useful for the theoretical understanding of the model, but the last four of them cannot be directly measured. In this section, we discuss the experimentally observable quantities and their relations to the parameters of the model.

#### 3.1 The total mixing

The formula (2.2) establishes the basis for experimental searches of the HNLs. It shows that an amplitude of a process involving HNL  $N_I$  is equal to the analogous amplitude involving active neutrino  $\nu_\alpha$  multiplied by  $\Theta_{\alpha I}$ .

In order to understand, how weakly HNLs are coupled to the SM in general, it is helpful to sum  $|\Theta_{\alpha I}|^2$  over flavours of active neutrinos and over  $I = 2, 3$ . This defines the total mixing

$$|U|^2 \equiv \sum_{\alpha I} |\Theta_{\alpha I}|^2 = \frac{1}{2M} \left[ (m_2 + m_3) (X_\omega^2 + X_\omega^{-2}) + \mathcal{O}\left(\frac{\Delta M}{M}\right) \right], \quad (3.1)$$

where  $m_{2,3}$  are masses of active neutrinos and the normal hierarchy (NH) of the active neutrino masses is assumed (the inverted hierarchy (IH) case can be obtained by replacing

$m_2 \rightarrow m_1, m_3 \rightarrow m_2$  in (3.1)). The total mixing (3.1) controls the amount of HNLs produced in an experiment and the lifetime of these HNLs.

### 3.2 Individual mixings

The total mixing (3.1) is useful to quantify interactions of the HNLs with the SM particles, however, it is not sufficient for determining sensitivity of experiments to the HNLs. Therefore we also consider individual, or flavoured, mixings.

To clarify the role of flavoured mixings, let us consider, e.g. the SHiP experiment [49, 63]. This is the beam dump-type experiment. An intense proton beam from the SPS accelerator hits the target. The main detector consists of a large empty decay volume with calorimeters and trackers at the end. In the SHiP set-up, HNLs are supposed to be produced mostly in decays of heavy mesons and the observational signatures consist of boosted charged particles originating from a vertex in the empty volume. The production is proportional to the partial decay width of a heavy meson into an HNL  $\Gamma(H \rightarrow N_I \ell_\alpha)$ , which is in turn proportional to the  $|\Theta_{I\alpha}|^2$ . It is important to note that the HNL production channels with different accompanying leptons  $\ell_\alpha$  are in principle distinguishable. In the SHiP, they could be discriminated if the mass of HNLs is close to upper bounds of kinematically allowed regions. Let us illustrate this in an example. Suppose that one observes a decay of an HNL with the mass exceeding  $m_{B_c} - m_\mu$  to a muon. This means that the HNL was produced along with an electron in the process  $B_c \rightarrow N_I e$  since the process  $B_c \rightarrow N_I \mu$  is kinematically forbidden.

The decay widths of HNLs are in turn proportional to  $|\Theta_{J\beta}|^2$ . The channels with charged leptons  $\ell_\beta$  in the final state are also distinguishable. In the example above the product of  $|\Theta_{I\alpha}|^2$  and  $|\Theta_{J\beta}|^2$  is important.

Therefore, individual mixings are phenomenologically relevant. Notice also that for the mass difference range which we are studying here the characteristic oscillation length is several orders of magnitude smaller than the length SHiP shielding and fiducial volume.<sup>3</sup> Namely, the oscillation length 100 m coincides to  $\sim 10^{-7}$  eV *physical* mass difference. Therefore for the lepton  $\ell_\alpha$  in the target and  $\ell_\beta$  in the detector one has to sum incoherently over  $I, J$ . So the total dependence on mixings is

$$\sum_{I,J=2,3} |\Theta_{I\alpha}|^2 \cdot |\Theta_{J\beta}|^2 = |U_\alpha|^2 \cdot |U_\beta|^2.$$

The individual mixings as functions of the parameters are given by

$$|U_\alpha|^2 \equiv \sum_{I=2,3} |\Theta_{I\alpha}|^2 = \frac{1}{2M} \left( |C_\alpha^+|^2 X_\omega^2 + |C_\alpha^-|^2 X_\omega^{-2} + \mathcal{O}\left(\frac{\Delta M}{M}\right) \right), \quad (3.2)$$

where the combinations  $C_\alpha^\pm$  for the NH case are

$$C_\alpha^\pm = iU_{\alpha 2}^{PMNS} \sqrt{m_2} \pm \xi U_{\alpha 3}^{PMNS} \sqrt{m_3} \quad (3.3)$$

---

<sup>3</sup>The case when the oscillations of HNLs are important will be addressed in a separate study.

and for the IH case

$$C_{\alpha}^{\pm} = iU_{\alpha 1}^{PMNS}\sqrt{m_1} \pm \xi U_{\alpha 2}^{PMNS}\sqrt{m_2}, \quad (3.4)$$

where  $U_{\alpha i}^{PMNS}$  with  $i = 1, 2, 3$  are the elements of the PMNS matrix (should not be confused with  $|U_{\alpha}|^2$ ).

#### 4 Cosmologically motivated values of mixings

In this section, we present our main results, namely, the values of the total and individual mixings of HNLs with active neutrinos for which the observed BAU can be explained by the  $\nu$ MSM. We describe how these results were obtained in a separate section 8.

The value of the BAU can be characterised in different ways. Throughout this work, we use the variable  $Y_B = n_B/s$ , where  $n_B$  is the baryon number density (particles minus antiparticles) and  $s$  is the entropy density. The observed value is  $Y_B^{obs} = (8.81 \pm 0.28) \cdot 10^{-11}$  [64]. For each set of the model parameters, we numerically find the value of  $Y_B$ . We are interested in the regions of the parameter space where one can reproduce the observed value  $Y_B^{obs}$ .

The regions of successful baryogenesis are shown in figure 1. In order to indicate how large can be the effect of the theoretical uncertainties in BAU computation, discussed in section 6, we show the borders of the regions where one can generate  $2 \cdot Y_B^{obs}$ , and  $Y_B^{obs}/2$ .

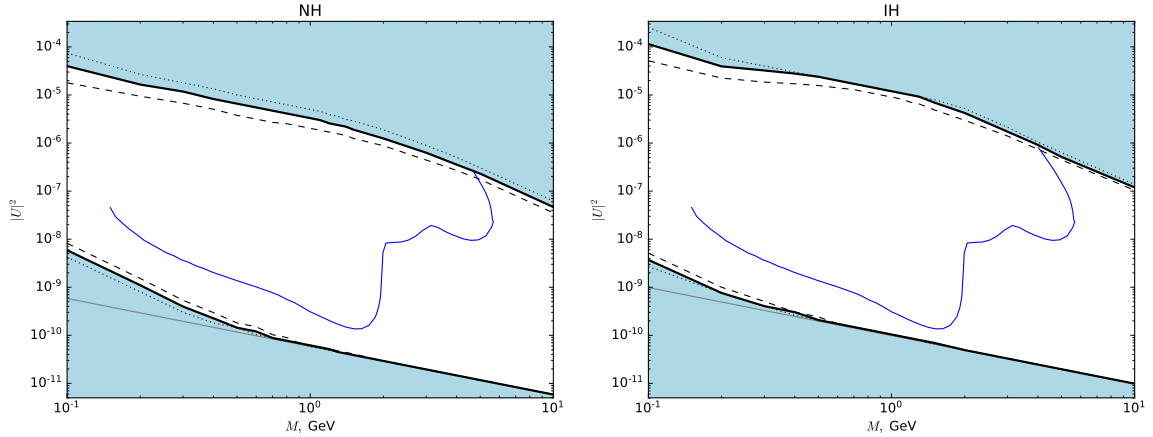


**Figure 1.** Within the white regions it is possible to reproduce the observed value of the BAU (black solid curves). The dashed and dotted curves demonstrate how large the possible theoretical uncertainties could be. Namely, the dashed curves correspond to the condition  $Y_B \geq 2 \cdot Y_B^{obs}$ , whereas the dotted lines correspond to  $Y_B \geq Y_B^{obs}/2$  accounting for the factor of 2 uncertainty in the computation of the BAU. The thin grey lines show the see-saw limit, i.e. it is impossible to obtain the correct masses of active neutrinos below these lines. The blue line shows the projected sensitivity of the SHiP experiment ref. [65] as presented in ref. [66]. *Left panel:* normal hierarchy, *right panel:* inverted hierarchy.

The cosmologically favoured region of the parameter space is larger for light HNLs than it was previously recognized (see also the discussion in section 9, in particular, figure 7). The fact that successful baryogenesis is possible for quite large values of the mixings rises



the question about the upper bounds of sensitivity of the direct detection experiments. To illustrate this point, we estimate the lifetime of an HNL using expressions for the decay rates of HNLs from ref. [67]<sup>4</sup>. For instance, let us consider an HNL with the mass  $M = 5$  GeV and mixings close to the upper boundary in figure 1. For such an HNL the lifetime is of the order of  $5 \cdot 10^{-9}$  s. Estimating the gamma factor to be  $\simeq 10$  we see that the decay length in the lab frame is less than 15 m. This implies that, e.g., in the SHiP experiment this HNL will decay well before the detector. Therefore it might be interesting to revisit the current experimental bounds on HNLs.

Let us note in passing that there also exist bounds from the Big Bang nucleosynthesis [23, 60, 67]. The question of the derivation of such bounds has been addressed in details for HNLs with the mass below 140 MeV in ref. [62]. For heavier Majorana HNLs an accurate derivation is still missing.

Results for the individual mixings  $|U_\alpha|^2$  and products  $|U_\alpha| \cdot |U_\beta|$  are presented in figures 2 and 3.

## 5 Open access datasets

In the previous section we have presented the boundaries of the regions where all observed BAU can be addressed within the  $\nu$ MSM in terms of various combinations of the mixings of HNLs and active neutrinos. However, the parameter space of the  $\nu$ MSM is not completely determined by the plots presented above, and there are more hidden parameters. These parameters can be essential for experimental searches for different signatures, and, e.g. it is interesting to know branching ratios, such as  $N \rightarrow \pi \ell_\alpha$  determined by  $U_e : U_\mu : U_\tau$ . For instance, what ratios of  $U_e : U_\mu : U_\tau$  are possible for some point in the allowed region of figure 2 or 3? This information is crucial to determine the decay length and branching ratios of various detection channels. In order to fill in this gap, we publish several datasets [68].

- Upper and lower boundaries of the  $M - |U|^2$  region where successful baryogenesis is possible as functions of the common mass of HNLs. Note that these lines correspond to the region where one can obtain  $Y_B \geq Y_B^{obs}$ .
- The dataset of models with successful baryogenesis. The value of the BAU for every model (a parameter set) in this list lies in the range  $[Y_B^{obs}/2, 2 \cdot Y_B^{obs}]$ . Note that the value of the  $Y_B$  is recorded for each parameter set so one can easily perform another cuts. The models of this dataset can be used to perform detailed Monte Carlo simulations of the experiments because they contain all necessary information  $(M, |U_e|^2, |U_\mu|^2, |U_\tau|^2)$ .
- The dataset of models leading to various values of the BAU. Even though not all of these models provide a correct value of the BAU, they can be used to compare different theoretical approaches.
- Selected benchmark points are gathered in appendix D.

---

<sup>4</sup>Note that this work was updated recently [66] with new channels added, so our estimate is conservative.

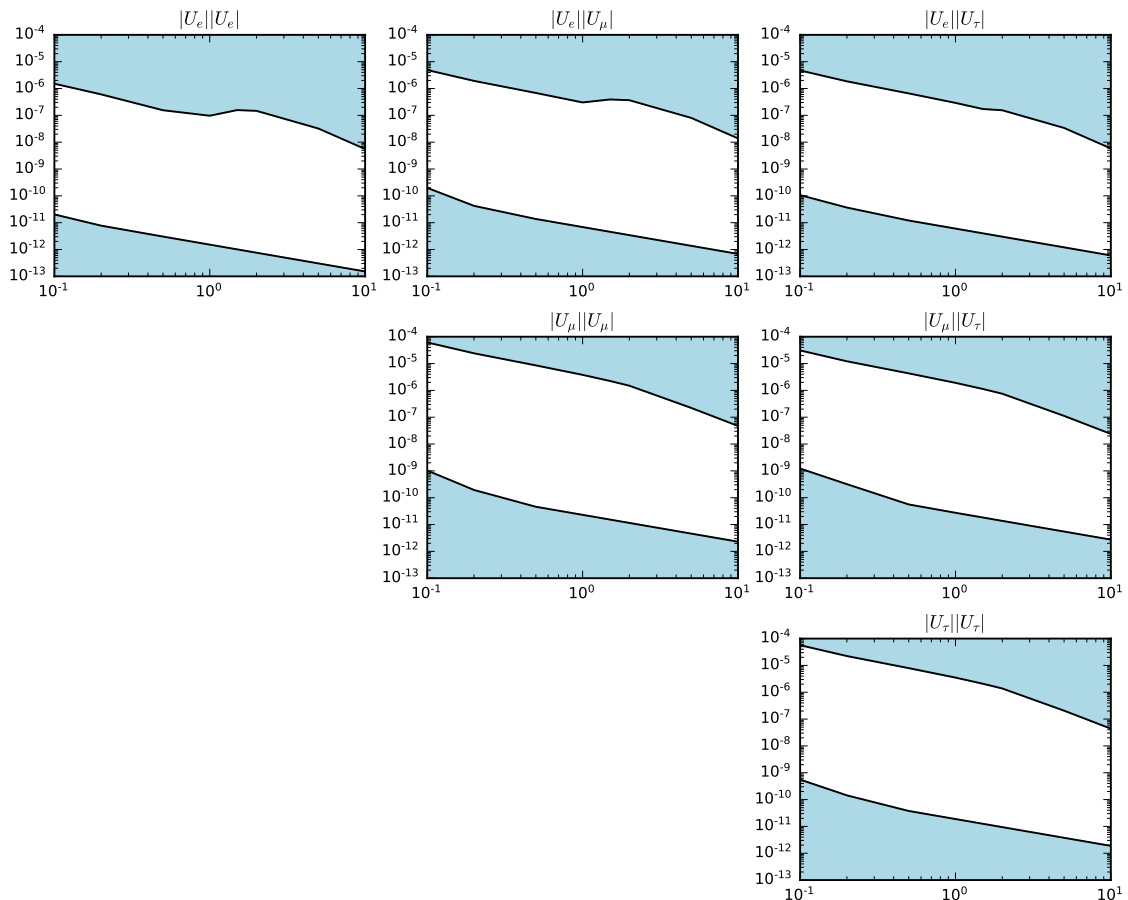


**Figure 2.** Cosmologically motivated regions of the individual mixings  $|U_\alpha|^2$  and products  $|U_\alpha| \cdot |U_\beta|$ . Within the white regions it is possible to reproduce the observed value of the BAU. The common mass is shown in the horizontal axes, whereas the vertical axes show the corresponding product of mixings. NH case.

## 6 Generation of the baryon asymmetry

### 6.1 Kinetic equations

In this section, we discuss the machinery of baryogenesis in the  $\nu$ MSM. We present the kinetic equations which form the basis of the numerical analysis of this paper. These equations possess the same generic structure as those used in refs. [8, 15, 23, 32–34]. However, several important improvements are incorporated. These are: *(i)* splitting of the rates to fermion number conserving and fermion number violating ones [36, 37]; *(ii)* accounting for neutrality of the electroweak plasma (this requirement was added to kinetic equations in [24]) and *(iii)* non-instantaneous freeze-out of sphalerons studied in [38, 40]. The rates entering the kinetic equations are updated using the recent results of ref. [69]. The only remaining source of possible uncertainties is the averaging procedure described below.

The detailed derivation of the equations is presented in appendix B. Here we start from the system of kinetic equations, introduce an ansatz which allows us to integrate

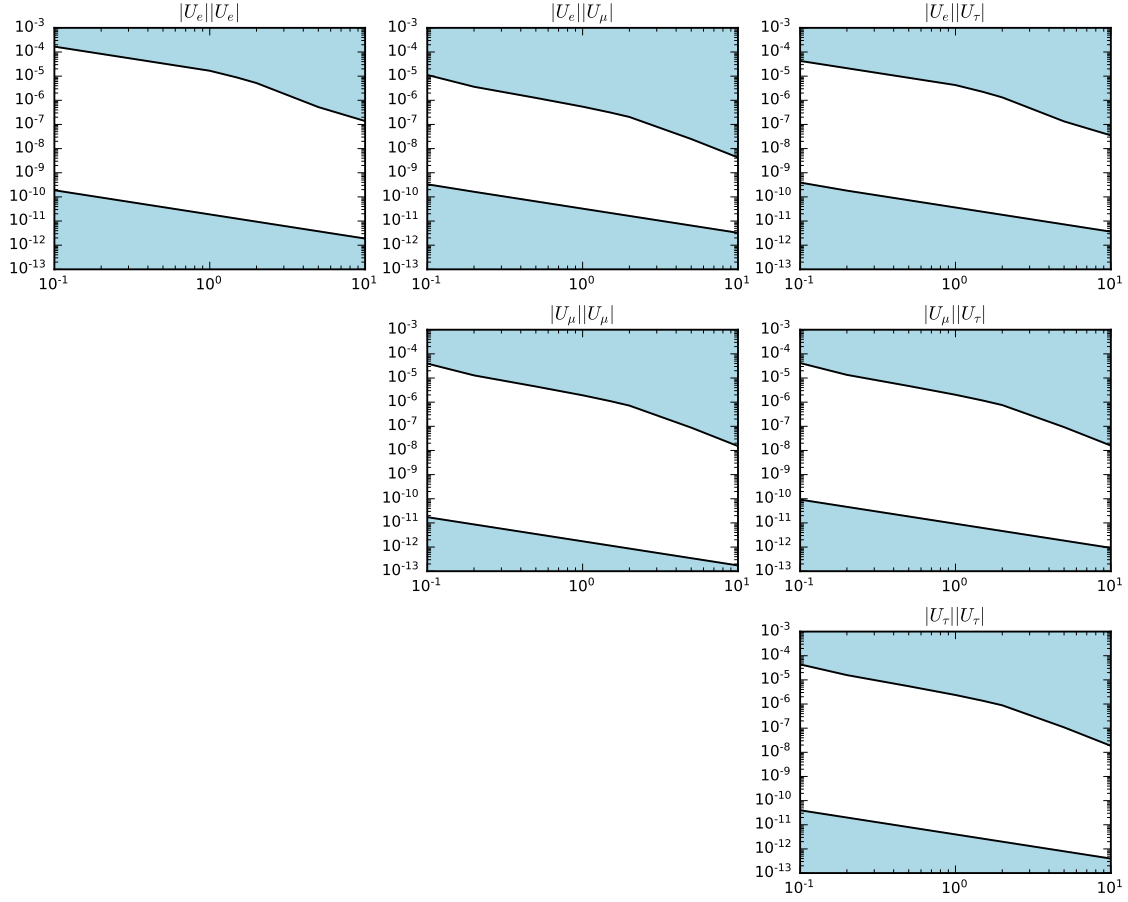


**Figure 3.** Cosmologically motivated regions of the individual mixings  $|U_\alpha|^2$  and products  $|U_\alpha| \cdot |U_\beta|$ . Within the white regions it is possible to reproduce the observed value of the BAU. The common mass is shown in the horizontal axes, whereas the vertical axes show the corresponding product of mixings. IH case.

these equations over the momentum and show how the gradual freeze-out of the sphaleron processes can be accounted for. The subscripts 2 and 3 are inherited from the  $\nu$ MSM and used to distinguish two HNLs participating in the generation of the BAU.

We are interested in coherent oscillations of HNLs and their interactions with leptons. The HNLs  $N_2$  and  $N_3$  are Majorana fermions with two helicity states each. Helicities are used to distinguish particles from anti-particles. We assign positive fermion number to HNLs with positive helicity and vice versa. Distribution functions and correlations of two HNLs are combined into matrices of density  $\rho_N$  ( $\rho_{\bar{N}}$  for antiparticles). The kinetic equations for leptons are presented in terms of the densities of the  $\Delta_\alpha = L_\alpha - B/3$ , where  $L_\alpha$  are the lepton numbers and  $B$  is the total baryon number. These combinations are not affected by the fast sphaleron processes and change only due to interactions with HNLs, therefore their derivatives are equal to the derivatives of the lepton number densities  $n_{L_\alpha}$ . Here we present the equations determining the generation of asymmetries in terms of  $\Delta_\alpha$ . In the next subsection, these asymmetries are related to the BAU. The system of kinetic

equations reads

$$i \frac{dn_{\Delta_\alpha}}{dt} = -2i \frac{\mu_\alpha}{T} \int \frac{d^3k}{(2\pi)^3} \Gamma_{\nu_\alpha} f_\nu (1 - f_\nu) + i \int \frac{d^3k}{(2\pi)^3} \left( \text{Tr}[\tilde{\Gamma}_{\nu_\alpha} \rho_{\bar{N}}] - \text{Tr}[\tilde{\Gamma}_{\nu_\alpha}^* \rho_N] \right), \quad (6.1a)$$

$$i \frac{d\rho_N}{dt} = [H_N, \rho_N] - \frac{i}{2} \{ \Gamma_N, \rho_N - \rho_N^{eq} \} - \frac{i}{2} \sum_\alpha \tilde{\Gamma}_N^\alpha \left[ 2 \frac{\mu_\alpha}{T} f_\nu (1 - f_\nu) \right], \quad (6.1b)$$

$$i \frac{d\rho_{\bar{N}}}{dt} = [H_N^*, \rho_{\bar{N}}] - \frac{i}{2} \{ \Gamma_N^*, \rho_{\bar{N}} - \rho_{\bar{N}}^{eq} \} + \frac{i}{2} \sum_\alpha (\tilde{\Gamma}_N^\alpha)^* \left[ 2 \frac{\mu_\alpha}{T} f_\nu (1 - f_\nu) \right]. \quad (6.1c)$$

In (6.1)  $f_\nu = 1/(e^{k/T} + 1)$  is the Fermi-Dirac distribution function of a massless neutrino. The effective Hamiltonian describing the coherent oscillations of HNLs is

$$H_N = H_0 + H_I, \quad H_0 = -\frac{\Delta M M}{E_N} \sigma_1, \quad H_I = h_+ \sum_\alpha Y_{+,\alpha}^N + h_- \sum_\alpha Y_{-,\alpha}^N, \quad (6.2)$$

where  $E_N = \sqrt{k_N^2 + M^2}$  and  $\sigma_1$  is the first Pauli matrix.

The damping rates are

$$\begin{aligned} \Gamma_N &= \Gamma_+ + \Gamma_-, \quad \Gamma_+ = \gamma_+ \sum_\alpha Y_{+,\alpha}^N, \quad \Gamma_- = \gamma_- \sum_\alpha Y_{-,\alpha}^N, \\ \Gamma_{\nu_\alpha} &= (\gamma_+ + \gamma_-) \sum_I h_{\alpha I} h_{\alpha I}^*. \end{aligned} \quad (6.3)$$

The communication terms, describing the transitions from HNLs to active neutrinos, are

$$\tilde{\Gamma}_N^\alpha = -\gamma_+ Y_{+,\alpha}^N + \gamma_- Y_{-,\alpha}^N, \quad \tilde{\Gamma}_{\nu_\alpha} = -\gamma_+ Y_{+,\alpha}^\nu + \gamma_- Y_{-,\alpha}^\nu. \quad (6.4)$$

In the expressions above the subscripts  $+$  and  $-$  refer to the fermion number conserving and violating quantities correspondingly. The functions  $h_\pm$  and  $\gamma_\pm$  depend only on kinematics (i.e. on the common mass of HNLs). These functions have to be determined over the whole temperature region of the interest. This region includes both symmetric and Higgs phases. In the Higgs phase, the rates can be split—in terms of ref. [28]—into “direct” and “indirect” contributions<sup>5</sup>. The direct contributions correspond to the processes where the Higgs field actually propagates. These reactions are also present in the symmetric phase. The processes with the Higgs field replaced by its temperature dependent expectation value give rise to the indirect contributions. These indirect contributions are crucial at low temperatures. As

---

<sup>5</sup>Note that this separation is gauge dependent [28]. It is the sum of direct and indirect contributions which is gauge independent.

we show below, they are also important for the baryogenesis.

$$\begin{aligned}
h_+ &= h_+^{\text{direct}} + \frac{2\langle\Phi\rangle^2 E_\nu (E_N + k)(E_N + E_\nu)}{kE_N \left(4(E_N + E_\nu)^2 + \gamma_{\nu(+)}^2\right)}, \\
h_- &= h_-^{\text{direct}} + \frac{2\langle\Phi\rangle^2 E_\nu (E_N - k)(E_N - E_\nu)}{kE_N \left(4(E_N - E_\nu)^2 + \gamma_{\nu(-)}^2\right)}, \\
\gamma_+ &= \gamma_+^{\text{direct}} + \frac{2\langle\Phi\rangle^2 E_\nu (E_N + k)\gamma_{\nu(+)}}{kE_N \left(4(E_N + E_\nu)^2 + \gamma_{\nu(+)}^2\right)}, \\
\gamma_- &= \gamma_-^{\text{direct}} + \frac{2\langle\Phi\rangle^2 E_\nu (E_N - k)\gamma_{\nu(-)}}{kE_N \left(4(E_N - E_\nu)^2 + \gamma_{\nu(-)}^2\right)},
\end{aligned} \tag{6.5}$$

In eqs. (6.5) the first and second terms represent the direct and indirect contributions respectively. Below we discuss the direct contributions, the neutrino dumping rates  $\gamma_{\nu,(\pm)}$ , and the neutrino potential in medium  $b$  entering eq. (6.5) through  $E_\nu = k - b$ . The derivation of the indirect contributions is presented in Appendix B.

The direct contributions to the effective Hamiltonians  $h_\pm$  come from the real part of HNL's self energy  $\not{Z}_N(p) = \not{p}\alpha + \not{p}\beta$ . Namely, one has<sup>6</sup>

$$h_\pm^{\text{direct}} = \frac{1}{2p^0} (\text{Re } \beta(p^0 \pm p) \mp m_N^2 \text{Re } \alpha). \tag{6.6}$$

At high-temperature limit the function  $h_+$  reproduces the standard Weldon correction  $T^2/(8k)$  [70]. If one neglects  $\alpha$ , which is numerically insignificant, the  $h_-$  is suppressed compared to  $h_+$  by a factor  $M_N^2/p^2$ . Thus  $h_-$  is very small in the symmetric phase and, at the same time, the indirect contribution dominates in the Higgs phase. In our numerical computations we use the real part of the HNL safe energy calculated in ref. [28].

We now move to the direct contributions  $\gamma_\pm^{\text{direct}}$ . They originate from  $1 \leftrightarrow 2$ ,  $2 \leftrightarrow 2$ , and  $1 + n \leftrightarrow 2 + n$  processes. The latter two require proper resummations [18, 37]. Fermion number conserving rate comes mainly from the  $2 \leftrightarrow 2$  scatterings. Another contribution to  $\gamma_+^{\text{direct}}$  comes from  $1 + n \leftrightarrow 2 + n$ . Fermion number violating rate comes from the  $1 + n \leftrightarrow 2 + n$  processes (note that  $2 \leftrightarrow 2$  scatterings do not contribute to  $\gamma_-^{\text{direct}}$ ). For our numerical analysis we use  $\gamma_\pm^{\text{direct}}$  kindly provided by the authors of ref. [69]. It is important to stress that in ref. [69] the temperature of the electroweak crossover  $T_c$  has been extracted from the one loop correction to the Higgs potential. Computed this way,  $T_c \simeq 150$  GeV [28], whereas the non-perturbative result is  $T_c^{\text{NP}} \simeq 160$  GeV [71, 72]. Since we are using the rates from ref. [69], the crossover temperature is set to  $T_c \simeq 150$  GeV. We also implement one-loop running of the couplings following the approach of ref. [73].

The last two ingredients entering (6.5) are the neutrino dumping rates  $\gamma_{\nu,(\pm)}$  and the neutrino potential in the medium  $b$ . The function  $b$  can be calculated following, e.g. refs. [74,

---

<sup>6</sup>Note that the term proportional to  $\alpha$  has been omitted in ref. [69] since it is subleading. Here we keep it for completeness. Note also that according to the formal power counting of ref. [69] the contribution  $h_-^{\text{direct}}$  has to be omitted as well.

75]. The neutrino damping rates are related to its self energy  $\Sigma_\nu(k) = \not{k}(a + i\Gamma_k/2) + \not{u}(b + i\Gamma_u/2)$  as

$$\gamma_{\nu(+)} = \Gamma_u + 2k^0\Gamma_k, \quad \gamma_{\nu(-)} = \Gamma_u. \quad (6.7)$$

In the temperature region of interest, the neutrino damping rates are dominated by  $2 \leftrightarrow 2$  process mediated by soft gauge bosons. The calculation of these rates requires proper resummations [28]. We use analytical results presented in ref. [69].

The dependence on the Yukawa coupling constants factorises out from the rates (6.2)–(6.4). It is convenient to introduce the matrix of Yukawa couplings  $h_{\alpha I}$  related to the matrix  $F_{\alpha I}$  defined in (2.1) as follows

$$F_{\alpha I} = h_{\alpha J}[U_N^*]_{JI}, \quad U_N = \frac{1}{\sqrt{2}} \begin{pmatrix} -i & 1 \\ i & 1 \end{pmatrix}. \quad (6.8)$$

In terms of these couplings we have

$$\begin{aligned} Y_{+,\alpha}^N &= (Y_{+,\alpha}^\nu)^T = \begin{pmatrix} h_{\alpha 3}h_{\alpha 3}^* & -h_{\alpha 3}h_{\alpha 2}^* \\ -h_{\alpha 2}h_{\alpha 3}^* & h_{\alpha 2}h_{\alpha 2}^* \end{pmatrix}, \\ Y_{-,\alpha}^N &= (Y_{-,\alpha}^\nu)^T = \begin{pmatrix} h_{\alpha 2}h_{\alpha 2}^* & -h_{\alpha 3}h_{\alpha 2}^* \\ -h_{\alpha 2}h_{\alpha 3}^* & h_{\alpha 3}h_{\alpha 3}^* \end{pmatrix}. \end{aligned} \quad (6.9)$$

The relation between the number densities and the chemical potentials to leptons in eq. (6.1) has to take into account the neutrality of plasma. When the system is in equilibrium with respect to sphaleron processes, this relation reads

$$\mu_\alpha = \omega_{\alpha\beta}(T)n_{\Delta_\beta}, \quad (6.10)$$

where  $\omega_{\alpha\beta}(T)$  is the so-called susceptibility matrix, see, e.g. [28, 38]. In the symmetric phase its diagonal elements are  $\omega_{\alpha\alpha} = 514/(237T^2)$ , while the off-diagonal  $\omega_{\alpha\beta} = 40/(237T^2)$ ,  $\alpha \neq \beta$ . Note that relation (6.10) should be modified for temperatures below the  $T_{sph} \simeq 131.7$  GeV at which the sphalerons decouple [76]. Full expressions of the susceptibility matrices can be found in ref. [38].

The set (6.1) is a system of coupled integro-differential equations for each momentum mode of HNLs. Numerical solution of this system is a very complicated task [19, 40]. However, a certain ansatz could be made to simplify the system. Namely, let us assume that the momentum dependence of the distribution functions is the equilibrium one,  $\rho_X(k, t) = R_X(t)f_N(k)$ , where  $f_N(k)$  is the Fermi-Dirac distribution of the massive HNLs. Then it is possible to integrate the kinetic equations over the momentum and obtain a set of ordinary differential equations. This procedure is the main source of the theoretical uncertainty. The error can be estimated by comparing solutions of the averaged equations with solutions of the full set (6.1). This has been done first in ref. [19]. Results of this work indicate that the error in the value of the BAU doesn't exceed 40%. Authors of the recent study [40] have also solved the full system. They have found that the accurate result differs by a factor of 1.5 from the benchmark of ref. [33]. However, note that the equations of ref. [40] include effects that haven't been accounted for in ref. [33]. We have also tested the benchmark points

listed in [77] using the same neutrino oscillation data as in [40] and found a surprisingly good agreement for the most of the benchmark points. A file with the values of the BAU for all benchmark points could be found in [68]. In what follows we will be conservative and assume that the averaging can lead to a factor of two error.

Let us finally present the system of equations that we actually solve numerically. It is convenient to introduce the CP-even and CP-odd combinations  $\rho_+ \equiv (\rho_N + \rho_{\bar{N}})/2 - \rho_N^{eq}$ ,  $\rho_- \equiv \rho_N - \rho_{\bar{N}}$ . The averaged equations read

$$\begin{aligned}
\dot{n}_{\Delta_\alpha} &= -\text{Re} \bar{\Gamma}_{\nu_\alpha} \mu_\alpha \frac{T^2}{6} + 2i \text{Tr}[(\text{Im} \tilde{\Gamma}_{\nu_\alpha}) n_+] - \text{Tr}[(\text{Re} \tilde{\Gamma}_{\nu_\alpha}) n_-], \\
\dot{n}_+ &= -i[\text{Re} \bar{H}_N, n_+] + \frac{1}{2}[\text{Im} \bar{H}_N, n_-] - \frac{1}{2}\{\text{Re} \bar{\Gamma}_N, n_+\} - \frac{i}{4}\{\text{Im} \bar{\Gamma}_N, n_-\} \\
&\quad - \frac{i}{2} \sum (\text{Im} \tilde{\Gamma}_N^\alpha) \mu_\alpha \frac{T^2}{6} - S^{eq}, \\
\dot{n}_- &= 2[\text{Im} \bar{H}_N, n_+] - i[\text{Re} \bar{H}_N, n_-] - i\{\text{Im} \bar{\Gamma}_N, n_+\} - \frac{1}{2}\{\text{Re} \bar{\Gamma}_N, n_-\} \\
&\quad - \sum (\text{Re} \tilde{\Gamma}_N^\alpha) \mu_\alpha \frac{T^2}{6},
\end{aligned} \tag{6.11}$$

with the integrated rates defined as

$$\begin{aligned}
\bar{\Gamma}_{\nu_\alpha} &= \frac{6}{\pi^2} \int dk_c k_c^2 e^{k_c} f_\nu^2 \Gamma_{\nu_\alpha}, \quad \tilde{\Gamma}_{\nu_\alpha} = \frac{T^3}{2\pi^2} \frac{1}{n_N^{eq}} \int dk_c k_c^2 f_N \tilde{\Gamma}_{\nu_\alpha}, \\
\bar{H}_N &= \frac{T^3}{2\pi^2} \frac{1}{n_N^{eq}} \int dk_c k_c^2 f_N H_N, \quad \bar{\Gamma}_N = \frac{T^3}{2\pi^2} \frac{1}{n_N^{eq}} \int dk_c k_c^2 f_N \Gamma_N, \\
\tilde{\Gamma}_N^\alpha &= \frac{6}{\pi^2} \int dk_c k_c^2 e^{k_c} f_\nu^2 \tilde{\Gamma}_N^\alpha, \quad S^{eq} = \frac{T^3}{2\pi^2} \frac{1}{s} \int dk_c k_c^2 f_N \cdot \mathbf{1}_{2 \times 2}.
\end{aligned} \tag{6.12}$$

Equations (6.11) are formulated in a static universe. The expansion of the Universe can be accounted for by rewriting eqs (6.11) in terms of the so-called yields  $Y_X = n_X/s$ , where  $n_X$  is the number density of species  $X$  and  $s$  is the entropy density which is conserved in the co-moving volume. For the numerical computations we use  $s(T)$  calculated in refs. [71, 78].

## 6.2 Gradual freeze-out of sphalerons

The asymmetry generated in the lepton sector is communicated to the baryon sector by the sphaleron processes. As long as these processes are fast compared to the rate of the asymmetry generation, the following equilibrium relation holds [79, 80]

$$Y_{B^{eq}} = -\chi(T) \sum_\alpha Y_{\Delta_\alpha}, \quad \chi(T) = \frac{4(27(\sqrt{2}\langle\Phi\rangle/T)^2 + 77)}{333(\sqrt{2}\langle\Phi\rangle/T)^2 + 869}, \tag{6.13}$$

where  $\langle\Phi\rangle$  is the Higgs vacuum expectation value, which is equal to 174.1 GeV at zero temperature. However, as was demonstrated in ref. [38], a deviation from the equilibrium with respect to sphalerons happens at temperatures around 140 GeV, i.e., before the freeze-out. It was also shown that the errors stemming from the usage of the equilibrium formula can exceed an order of magnitude. To overcome this problem, one can implement the

method suggested in ref. [38]. Namely, one solves the kinetic equation for the baryon number [80, 81]

$$\dot{Y}_B = -\Gamma_B(Y_B - Y_{B^{eq}}), \quad (6.14)$$

where for the three SM generations

$$\Gamma_B = 3^2 \cdot \frac{869 + 333(\sqrt{2}\langle\Phi\rangle/T)^2}{792 + 306(\sqrt{2}\langle\Phi\rangle/T)^2} \cdot \frac{\Gamma_{diff}(T)}{T^3}, \quad (6.15)$$

where  $Y_{B^{eq}}$  is given by eq. (6.13) and  $\sum_\alpha Y_{\Delta_\alpha}$  is calculated from the main system (6.11). It is enough to solve eq (6.14) starting from  $T = 150$  GeV.

This finishes the presentation of the kinetic equations. To summarize, our equations incorporate all physical effects that are relevant for the range of HNL masses considered here. The only source of errors is the momentum averaging of the kinetic equations. Based on the previous studies [19, 40], we conservatively estimate that these errors do not exceed a factor of two.

### 6.3 Physics of asymmetry generation

Before solving eqs.(6.11) numerically, we briefly discuss the physics of the asymmetry generation. There are several important temperature scales. One of them is the already mentioned sphaleron freeze-out temperature  $T_{sph} \simeq 131.7$  GeV [76]. The lepton asymmetry generated at temperatures lower than  $T_{sph}$  does not affect the final value of  $Y_B$ .

Second scale is a temperature at which the HNLs enter thermal equilibrium,  $T_{in}$ . This temperature can be determined from the condition  $\bar{\Gamma}_N(T_{in})/H(T_{in}) \simeq 1$ , where  $H(T)$  is the Hubble rate and we take the largest eigenvalue of the matrix  $\bar{\Gamma}_N(T_{in})$ . The Hubble rate during radiation-dominated epoch is  $H(T) = T^2/M_{Pl}^*$ , where  $M_{Pl}^* = \sqrt{90/(8\pi^3 g_*)} M_{Pl}$ ,  $g_*$  is the effective number of relativistic degrees of freedom.

Another important scale is the so-called oscillation temperature,  $T_{osc}$ . Coherent oscillations of the HNLs play the crucial role in the generation of the individual lepton asymmetries. In fact, they provide a CP-even phase, which, being combined with the CP-odd phase from Yukawas, leads to the generation of the individual asymmetries, see, e.g. the discussion in ref. [15]. This mechanism becomes efficient around the first oscillation. The temperature at which the first oscillation takes place can be estimated as [8, 13]

$$T_{osc} \simeq \left( \frac{\delta M M M_{Pl}^*}{3} \right)^{1/3}, \quad (6.16)$$

where  $\delta M$  is the physical mass difference. This mass difference is the splitting between two eigenvalues of the effective Hamiltonian (6.2). Since the asymmetry generation is efficient at  $T$  around  $T_{osc}$ , one can roughly estimate the lower bound on the  $\delta M$  by requiring  $T_{osc} > T_{sph}$ .

Let us consider two cases:

- $T_{in} < T_{sph}$



This regime is sometimes referred to as *oscillatory*. In this case the kinetic equations could be solved perturbatively [8, 13] if also  $T_{osc} > T_{Sph}$ .<sup>7</sup> Late thermalization implies that Yukawa couplings are relatively small. In terms of the parameters listed in table 1, this regime is realized if the value of  $|\text{Im}\omega|$  is small.

- $T_{in} \geq T_{Sph}$

In this case, the dampings of the generated asymmetries are efficient, so this scenario is referred to as *strong wash-out regime*. Yukawa couplings must be relatively large, this can be in agreement with the oscillation data if  $|\text{Im}\omega|$  is large as well. Sizeable damping causes a wash-out of asymmetries before the freeze-out of sphaleron processes. However, the production of HNLs and interactions with left-handed leptons at high temperatures are also enhanced, so the asymmetry generation is more efficient. In order to account for all relevant processes, the kinetic equations have to be solved numerically.

## 7 Numerical analysis of the kinetic equations

Equations (6.11) together with (6.13) or (6.14) allow one to determine the value of the BAU for each parameter set in table 1. For most values of the parameters, the equations (6.11) have to be solved numerically. In this section, we discuss the procedure of solving these equations and demonstrate how the improvements in the equations influence the results.

### 7.1 The procedure for numerical solution of the equations

First of all, it is necessary to determine initial conditions. Right after the inflation the baryon and lepton numbers of the Universe as well as number densities of HNLs are equal to zero.<sup>8</sup> Thus we start from the vanishing  $Y_-(T_0) \equiv n_-(T_0)/s(T_0)$  and  $Y_{\Delta_\alpha}(T_0)$ . According to the definition of  $\rho_+$ , at initial stage  $Y_+(T_0) = -n^{eq}(T_0)/s(T_0)$ , where  $n^{eq}(T)$  is an equilibrium number density of a fermion with mass  $M$ .

The appropriate initial temperature can be specified on physical grounds. As we have discussed, the asymmetry generation starts around the temperature of the first oscillation,  $T_{osc}$ . We have checked numerically that no significant asymmetry is generated at the temperature  $10 \cdot T_{osc}$ , i.e. much before the onset of oscillations. Therefore we take  $T_0 = 10 \cdot T_{osc}$  if  $10 \cdot T_{osc} > 10^3$  GeV, or  $T_0 = 10^3$  GeV otherwise.

Now, having set up the initial conditions, we can solve equations (6.11). It is convenient to implement them using  $z = \log(M/T)$  as a variable. Even though the problem is reduced to the solution of the set of 11 ordinary differential equations (ODE) by means of averaging (6.12), it still remains challenging. The reason is that significantly different time scales are present in the system (6.11). Appropriate stiff ODE solvers, such as LSODA [82], can handle our equations quite efficiently. However, the integration time can be reduced further. Notice that the effective Hamiltonian entering equations (6.1) can be decomposed

---

<sup>7</sup>Note that when the fermion number violating effects are introduced, the total asymmetry is generated at order  $F^4$ .

<sup>8</sup>The effect of the initial asymmetry in the HNL sector has been studied in ref. [35].

as  $H_N = H_0 + H_I$ , where  $H_0 = -\Delta M M \sigma_1 / E_N$ . Therefore, we can move to the ‘interaction picture’ with respect to  $H_0$ . After this transformation, the equations can be solved using a non-stiff method.

The final value of the BAU is founded by solving eq. (6.14). This ensures that the value of the BAU is not affected by the assumption of an instantaneous freeze-out of sphalerons.

In order to find an appropriate method we have implemented equations (6.11) in the Python programming language. The SciPy library [83] allows one to use several different ODE solvers. We have found that the most efficient (in terms of the number of calls of the r.h.s.) one for our purposes is the LSODE [82]. The equations were then coded in the Fortran 77/95 along with the native Fortran implementation of the LSODE [84]. Note that for the successful integration it is important to carefully tune the parameters of the solver (such as absolute and relative tolerances for each variable).

We have also implemented the same system of kinetic equations in Mathematica [85]. This allowed us to validate the results obtained using the Fortran code. However, since the computation of r.h.s. takes much longer, the overall computation time is also very large. The Fortran realization outperforms the Mathematica one by more than four orders of magnitude.

The whole computation of the BAU for a single set of the parameters takes from  $\simeq 0.05$  sec in the oscillatory regime (approximately  $|\text{Im} \omega| < 2$ ) to  $\simeq 1.0$  sec in the strong wash-out regime (approximately  $|\text{Re} \omega| > 5.5$ ). The very efficient numerical procedure allows performing a comprehensive study of the parameter space.

## 7.2 Analysis of the equations

Before presenting the phenomenologically relevant results it is instructive to study the outcome of the improvements of the kinetic equations. First of all, it is interesting to see what values of mass splitting  $\Delta M$  and  $X_\omega$  can lead to a successful baryogenesis. In figure 4 we show the regions in the  $X_\omega - \Delta M$  plane where the value of the  $Y_B \geq Y_B^{\text{obs}}$  can be generated. To obtain this plot we have fixed the phases to the following values

$$\text{NH: } \delta = \pi, \quad \eta = 3\pi/2, \quad \text{Re} \omega = \pi/4, \quad (7.1a)$$

$$\text{IH: } \delta = 0, \quad \eta = \pi/2, \quad \text{Re} \omega = \pi/4. \quad (7.1b)$$

This choice of phases maximizes the value of  $|Y_B|$  in the strong wash-out regime (see more detailed discussion in section 8). Note that since the values of Dirac and Majorana phases were fixed and only  $\text{Im} \omega$  was varied, the contours are not symmetric. In all cases the positive  $\text{Im} \omega$  (large  $X_\omega$ ) gives larger BAU, as can be seen from figure 4.

The blue horizontal line in figure 4 indicates the zero-temperature Higgs contribution to the physical mass difference  $\delta M$  in the limit  $\Delta M/M \rightarrow 0$ . Below this line the Higgs contributions to the physical mass difference dominates, whereas above the line, the physical mass difference is mostly determined by the Majorana mass difference. This means that  $\delta M$  cannot be much smaller than  $\Delta M$  in the region above the line and  $\delta M$  cannot be much smaller than the Higgs contribution below the line. Smaller values of  $\delta M$ —which

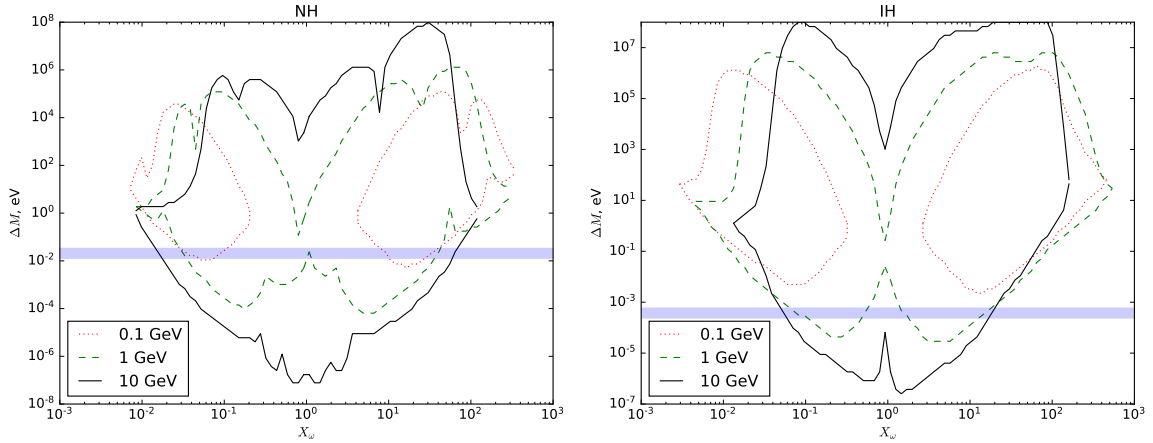


**Figure 4.** Allowed region in the  $X_\omega - \Delta M$  plane obtained for the fixed values of the phases (8.1). It is possible to generate  $Y_B \geq Y_B^{obs}$  within the corresponding regions. Common masses of the HNLs are fixed to be equal to 0.1, 1.0, 10 GeV. The blue horizontal line indicates the zero-temperature Higgs contribution to the physical mass difference  $\delta M$  in the limit  $\Delta M/M \rightarrow 0$ .

are interesting, e.g. for studies of resolvable HNL oscillations at the SHiP experiment—are only possible if there is a cancellation between  $\Delta M$  and the Higgs contribution. This cancellation can happen only close to the blue line.

It is also important to understand the role of the improvements that we consider. We want to address the questions: (i) what is the effect of the fermion number violating rates on the final value of the BAU; (ii) what is the effect of considering the Higgs phase; (iii) what is the effect of susceptibilities; (iv) what is the effect of the gradual decoupling of the sphalerons. In order to answer the first question, we effectively switch off fermion number violating processes in our kinetic equations. It is possible because the fermion number conserving and fermion number violating processes are neatly separated in eqs.(6.2), (6.3) and (6.4). So we can set  $\gamma_- = h_- = 0$  for the whole range of temperatures. In order to model the absence of the Higgs phase at temperatures down to 130 GeV we put  $\langle \Phi(T) \rangle = 0$ . We consider the NH case and two different values of the common mass, 1 GeV and 10 GeV. The phases are fixed to the values (7.1a). We present the results in figure 5. In order to see how accounting for the charge neutrality of plasma modifies the results we replace the susceptibility matrix in (6.10) by a diagonal one. In figure 6 we compare results with and without susceptibilities. One can see that the effect is quite sizeable. In the same figure we demonstrate the results with and without careful treatment of sphalerons.

Inspecting figures 5 and 6 one can arrive at the following conclusions.

- Fermion number violating rates.  
Accounting for the fermion number violation increases the  $Y_B$ . See figure 5, green dashed lines.
- Broken phase.  
Equations without the fermion number violation solved under the assumption that the Higgs vacuum expectation value is zero at all temperatures above the  $T_{sph}$  lead

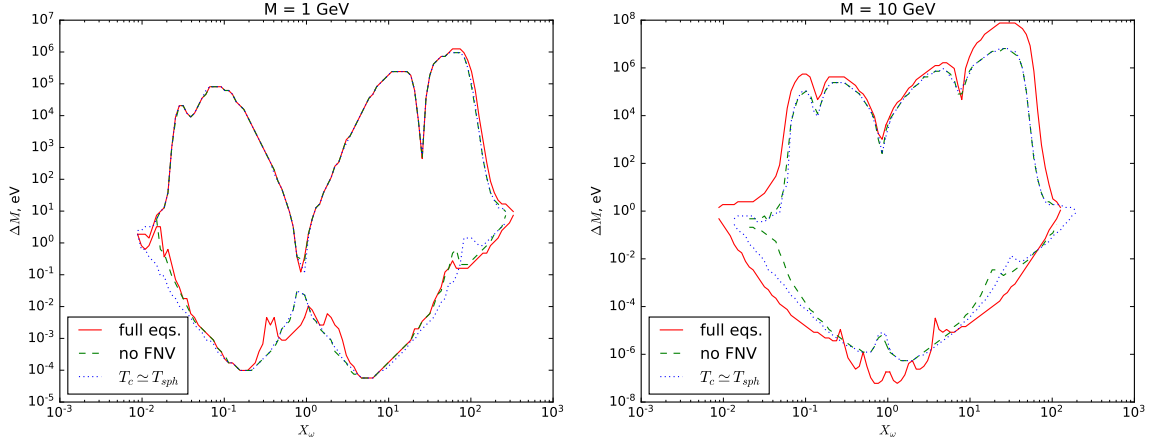


**Figure 5.** Red, solid line – full kinetic equations (6.11). No fermion number violation – green, dashed lines. Blue, dotted lines correspond to an assumption,  $T_{\text{EWPT}} \simeq T_{\text{sph}}$ , which has been used in a number of previous works so far. *Left panel*, common mass  $M = 1$  GeV. *Right panel*, common mass  $M = 10$  GeV.

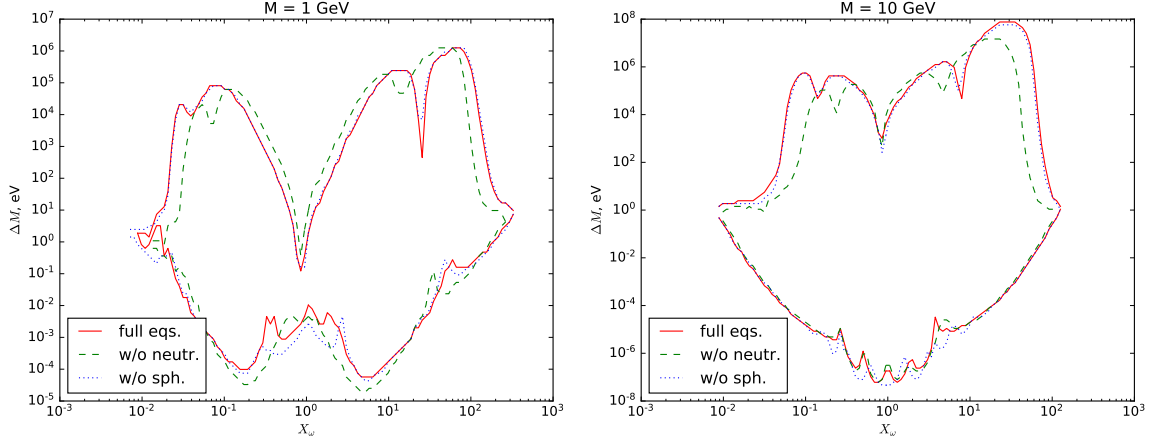


**Figure 6.** Comparing the kinetic equations with accurate susceptibilities and accurate treatment of sphalerons (red curve), with diagonal susceptibilities (no plasma neutrality) (green dashed curve) and with the instantaneous freeze-out of sphalerons (blue dotted curve). The same choice of phases as in the previous figure. *Left panel*, common mass  $M = 1$  GeV. *Right panel*, common mass  $M = 10$  GeV.

to larger amount of the  $Y_B$  for heavy HNLs at large  $|\text{Im } \omega|$ . See figure 5, blue dotted lines.

- Neutrality of plasma.

Accounting for the neutrality of plasma by means of susceptibilities is important. The effect is stronger for lighter HNLs. See figure 6.

- Freeze-out of sphalerons.

The boundary of the allowed region in figure 6 is not sensitive to the method of

calculation of the BAU from the lepton asymmetry. In fact, if one is interested in the upper bounds on the mixings (large  $|\text{Im } \omega|$ ) the instantaneous freeze-out of sphalerons can be assumed. See figure 6.

## 8 Study of the parameter space

In this section, we describe how the study of the parameter space of the model have been performed. Our strategy is a direct sampling of the parameters defining the theory. In subsection 8.1 we fix specific values of the phases  $\delta, \eta, \text{Re } \omega$  which maximize the generated asymmetry. In subsection 8.2 we sample the whole 6 dimensional parameter space.

### 8.1 Total mixing

In order to set the bound on the value of the total mixing (3.1) we need to find, for each value of the common mass, the largest value of  $|U|^2$ .

Since the value of  $|U|^2$  for a given mass depends only on  $\text{Im } \omega$ , one can marginalize over phases  $\delta, \eta, \text{Re } \omega$  and mass difference  $\Delta M$  and solve an optimization problem for  $\text{Im } \omega$ . The optimization problem consists of maximizing (or minimizing for negative values)  $\text{Im } \omega$  subject to  $Y_B \simeq Y_B^{obs}$ .

Several comments are in order. The value  $Y_B$  can be both positive or negative. If it is possible to obtain some value  $Y_B^1$  for some  $X_\omega$  and mass difference, then it is also possible to obtain  $-Y_B^1$  for the same  $X_\omega$  and  $\Delta M$  provided that the phase parameters in the model can vary freely. In what follows we would always take the absolute value  $|Y_B|$  of the computed BAU.

Next, it is important to clarify what does  $Y_B \simeq Y_B^{obs}$  actually mean. The kinetic equations that we solve contain an inherent error stemming from the assumption of equilibrium momentum dependence of density matrices. In order to account for this theoretical uncertainty we impose the following condition  $Y_B^{obs}/2 < |Y_B| < 2Y_B^{obs}$ .

In practice, it is easier to maximize  $|Y_B|$  for given values of  $\text{Im } \omega$  and  $M$ . If the maximal value of  $|Y_B|$  exceeds e.g.  $Y_B^{obs}$ , then it is also possible to generate a smaller value of asymmetry. One can iterate this procedure on a grid in  $\text{Im } \omega$  and  $M$  space. Then by interpolating  $|Y_B|$  as a function of  $\text{Im } \omega$  for a given  $M$  and finding roots of the equation  $|Y_B| = \kappa Y_B^{obs}$ ,  $\kappa = 0.5, 1, 2$ , one can find the upper and lower bounds on  $|U|^2$ . The case of  $\kappa = 2$  corresponds to the conservative assumption that the averaging procedure amounts to a twice larger asymmetry compared to the accurate treatment. Authors of ref. [40] have solved the full system of equations for several parameter points. Their results indicate that the averaged equations rather tend to underestimate the value of BAU. This case is indicated by  $\kappa = 0.5$ .

Maximizing  $|Y_B|$  with respect to  $\Delta M, \text{Re } \omega, \delta, \eta$  is a resource demanding task. It can be significantly simplified in the strong wash-out regime, i.e. for large values  $|\text{Im } \omega|$ . In this regime the value of the total asymmetry strongly depends on the difference in the damping rates of active neutrinos. For a given mass,  $X_\omega$  and mass difference the damping rates are controlled by Dirac and Majorana phases together with the real part of  $\omega$ . Note that a set of phases that maximizes the difference among these damping rates (and, the total lepton

asymmetry consequently) also minimizes (maximizes in the case of IH)  $|U_e|^2$ . We have used the following values<sup>9</sup>

$$\text{NH: } \delta = \pi, \quad \eta = 3\pi/2, \quad \text{Re } \omega = \pi/4, \quad (8.1a)$$

$$\text{IH: } \delta = 0, \quad \eta = \pi/2, \quad \text{Re } \omega = \pi/4. \quad (8.1b)$$

These choices of phases maximize one of the individual mixings  $U_\alpha$  (see Appendix A). For the NH case the phases (8.1a) maximize  $U_\mu$ , while for the IH case the phases (8.1b) maximize  $U_e$ . Since the phases are fixed, we need to find only the value of  $\Delta M$  which maximizes BAU at each point of the  $M - \text{Im } \omega$  grid. The upper bounds in figure 1 were obtained using the method described above. Let us stress that the same upper bounds can be obtained by the random sampling described in the next subsection. We have checked that two methods agree with each other. The lower bounds on the  $|U|^2$  obtained with the fixed phases (8.1) are not optimal, since the asymmetry is generated in the oscillatory regime. Therefore, the lower bounds in figure 1 are obtained by the direct sampling.

## 8.2 Individual mixings

The mixings  $|U_\alpha|^2$  depend on  $\delta$  and  $\eta$  through the elements of the PMNS matrix entering eqs. (3.3) or (3.4). Therefore it is no longer possible to solve a simple optimization problem, as was the case for  $|U|^2$ . However, our numerical routines solve kinetic equations for different values of parameters very efficiently. This allows us to perform a scan of the full parameter space.

The parameter space is sampled as follows. As was already mentioned, we are restricted to the discrete grid in the common mass  $M$  in the interval  $[0.1, 10.0]$  GeV. The rest of parameters we sample randomly, so that  $\log_{10} \Delta M, \text{Im } \omega, \text{Re } \omega, \delta, \eta$  are distributed uniformly in the intervals specified in table 1.<sup>10</sup> Note that according to eq. (A.22), the uniform distribution in  $\text{Im } \omega$  approximately coincides to a uniform distribution of  $|U_\alpha|^2$  in log-scale. However, in order to obtain the upper bounds more accurately, we also perform a flat sampling in the  $X_\omega$ . After computing the value of BAU for each point we select the points according to the criterion  $|Y_B| > Y_B^{obs}$ .

In order to plot figures 2 and 3 we have generated 2 800 000 points for each hierarchy type and selected only those points for which  $|Y_B| > Y_B^{obs}$ . We also have utilized these datasets to obtain the lower bounds and to cross check the upper bounds on the total mixing  $|U|^2$ .

## 9 Comparison with other works

Baryogenesis in the  $\nu$ MSM has attracted a lot of attention of the community in recent years. The first scan of the parameter space was performed in refs [21, 23]. Authors of

<sup>9</sup>The value  $\delta = 0$  for the IH case is incompatible with the recent  $3\sigma$  bounds of the NuFit 3.2 analysis. However, setting  $\delta = 354^\circ$  doesn't change the results presented here.

<sup>10</sup>Note that for the Dirac phase we have actually used the  $3\sigma$  interval from the NuFit 3.2 analysis. Namely,  $\delta \in [144^\circ, 374^\circ]$  in the NH case, and  $\delta \in [192^\circ, 354^\circ]$  in the IH case.

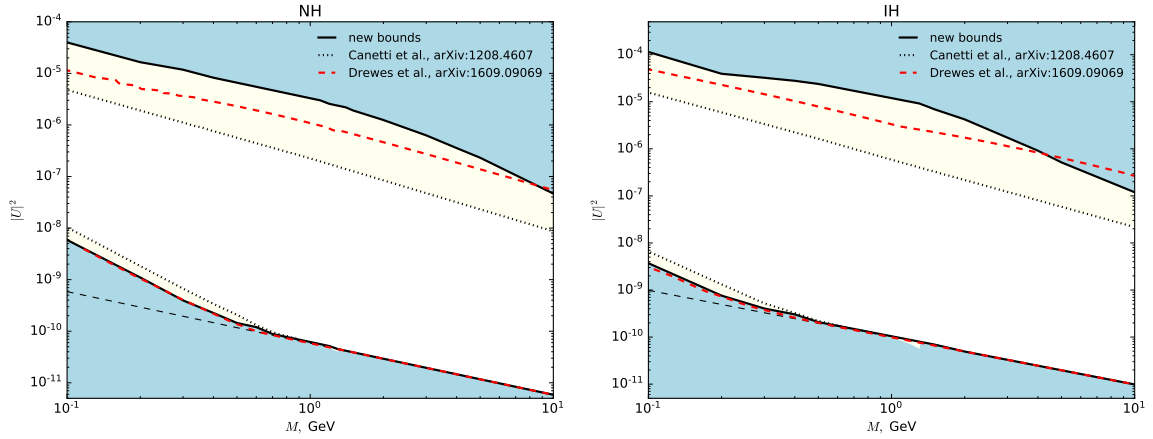


**Figure 7.** Comparison of the bounds from three different works. Our lower bounds (black solid lines) are obtained from the parameter sampling, whereas upper bounds are obtained for fixed phases.

ref. [24] have accounted for the neutrality of the electroweak plasma which leads to  $\mathcal{O}(1)$  corrections to the final asymmetry.

More recently, scans of the parameter space were performed by two groups, see refs. [32, 33]. The role of fermion number violating processes was clarified in refs [29, 36, 37, 86]. Implications of a non-instantaneous freeze-out of sphalerons were addressed in refs. [38, 40].

In what follows we list corresponding works.

#### L. Canetti, M. Drewes, T. Frossard, and M. Shaposhnikov [21, 23]

The first detailed study of the parameter space. Only the symmetric phase has been considered. Asymmetries in the leptonic sector were described by means of the chemical potentials, i.e. neutrality of the plasma has not been accounted for. The rates were underestimated by a factor of two (see table 2 below). In the scan of the parameter space the values of phases were fixed to non-optimal values. As a result, the allowed region of the parameter space is much smaller compared to what we have obtained in this work.

#### M. Drewes, B. Garbrecht, D. Gueter, and J. Klaric [32, 34]

In ref. [32] only the symmetric phase has been considered. The kinetic equations were generalized to the broken phase in ref. [34]. The rescaling of the parameters that simplified computations has been suggested in ref. [32]. The relation between leptonic chemical potentials and number densities accounting for the neutrality of the plasma has been implemented. This relation is analogous to eq (6.10), however it is valid only at large temperatures. In high-temperature limit this relation agrees with eq (6.10).

Note the persistent disagreement between the damping rate of the active neutrinos in ref. [32] and in our work (see discussion below).



**P. Hernández, M. Kekic, J. López-Pavón, J. Racker and J. Salvado [33]**

Only the symmetric phase has been considered. The neutrality of the plasma has been accounted for, however, apparently, the susceptibilities disagree with those in ref. [32] and with ours at high-temperature limit.<sup>11</sup>

The approach to the study of the parameter space is different from what we use in this work. The parameter space has been sampled by means of the Markov Chain Monte Carlo (MCMC) with certain priors. The cosmologically allowed regions of the parameter space were presented as contours 90% of all generated points. This method resulted in regions which are much smaller compared to what we have obtained in this work.

**S. Antusch, E. Cazzato, M. Drewes, O. Fischer, B. Garbrecht, D. Gueter et al [39]**

The scan of the parameter space of heavy HNLs ( $M > 5$  GeV). Fermion number violating processes have been accounted for in the symmetric phase. The parameter space has been sampled by means of the Markov Chain Monte Carlo (MCMC). However, the selection criteria is different from [33]. Namely, the models leading to  $Y_B^{obs} - 5\sigma_{Y_B^{obs}} < |Y_B| < Y_B^{obs} + 5\sigma_{Y_B^{obs}}$  were selected. This approximately corresponds to  $0.68 \cdot Y_B^{obs} < |Y_B| < 1.32 \cdot Y_B^{obs}$ . Let us emphasize that the uncertainties in the value of  $|Y_B|$  are theoretical, whereas the experimental uncertainty, characterized by  $\sigma_{Y_B^{obs}}$  is much smaller. This is the reason why throughout this work we consider a larger interval for  $|Y_B|$ .

**J. Ghiglieri and M. Laine [28, 37, 40, 69]**

There were no scans of the parameter space. However, a thorough derivation of all rates has been performed. The susceptibilities have been calculated accounting for the non-zero masses of the fermions in ref. [28]. The full non-averaged system has been solved for several benchmark points in ref. [40].

After the ArXiv version of this paper had been released, a new study [69] appeared. This work contains the most up-to-date determination of both fermion number conserving and violating rates in the whole temperature region relevant for baryogenesis. It was pointed out in ref. [69] that the  $2k\Gamma_k$  part of the  $\gamma_{\nu(+)}$  was missing in the ArXiv version of the present paper. In the current version of the paper we correct this point. We have also updated all rates entering the kinetic equations using the results of ref. [69].

---

<sup>11</sup> It is important to clarify that the matrix  $C_{\alpha\beta}$ , entering eq. (2.20) from ref. [33] agrees with our matrix  $\omega_{\alpha\beta}$  from eq. (6.10) provided that in ref. [33] the symbol  $\mu_\alpha$  denotes the chemical potential to left-handed leptons. Note that our  $\mu_\alpha$  are the chemical potentials to all leptons of flavour  $\alpha$ . Therefore,  $\mu_\alpha^{(ref. [33])} = \mu_\alpha^{(our)} - \mu_Y/2$ , where  $\mu_Y$  is the chemical potential to the hypercharge. We thank Jacopo Ghiglieri for pointing this out. However, once the chemical potentials are eliminated from the kinetic equations by means of eqs. (6.10) and (2.20) from ref. [33], the equations are actually different. Namely, in the r.h.s. of the equations the terms proportional to  $\sum_\beta \omega_{\alpha,\beta} Y_{\Delta_\beta}$  will appear. The matrices multiplying  $Y_{\Delta_\beta}$  are different in ref. [33] and in this work.



**T. Hambye and D. Teresi [29, 86]**

There were no scans of the parameter space. A role of fermion number violating Higgs decays has been discussed. The considerations of ref. [86] are limited to the Higgs decays and inverse decays. The rate of the fermion number conserving processes has been underestimated compared to the ones including  $2 \leftrightarrow 2$  scatterings. This can be seen, e.g. from figure 4 of ref. [37]. Therefore, a direct comparison between our study and ref. [86] is not straightforward.

It is important to note that the generic structure of kinetic equations is the same in all studies of the low-scale leptogenesis. Therefore it is possible to compare the rates in the kinetic equations independently of their derivation. In order to be able to compare refs [23, 32, 33, 40], we compute the corresponding rates at temperature  $T_{ref} = 10^3$  GeV. At this temperature the rates are dominated by lepton number conserving processes.

The production rate of HNLs, the communication term of HNLs, the damping term of the lepton asymmetries and their communication term can be described as

$$\bar{\Gamma}_N/h^2 = C_1 \cdot T, \quad (9.1)$$

$$\tilde{\bar{\Gamma}}_N/h^2 = C_2 \cdot T \quad (9.2)$$

$$\bar{\Gamma}_\nu/h^2 = C_3 \cdot T \quad (9.3)$$

$$\tilde{\bar{\Gamma}}_\nu/h^2 = C_4 \cdot T \quad (9.4)$$

where  $h^2$  is a symbolic representation of an appropriate product of Yukawa coupling constants for each term. The values of the coefficients  $C_i$  in considered works are summarized in table 2. Note that since authors of ref. [40] treat the momentum dependence exactly in their numerical computations, we cannot compare their rates, however the hierarchy among the rates and their values at  $k = 3T$  are the same as ours. Leaving aside ref. [23], one can

Article	$C_1$	$C_2$	$C_3$	$C_4$
This work	0.0097	0.0086	0.0086	0.0097
L. Canetti et al. [23]	0.005	0.005	0.005	0.005
M. Drewes et al. [32]	0.012	0.012	0.006	0.006
P. Hernández et al. [33]	0.0118	0.0069	0.0076	0.0130

**Table 2.** The coefficients of the rates in considered works.

see that the values of the coefficient  $C_1$  do agree with a reasonable precision. However, the values of the other coefficients differ roughly by a factor of two from work to work. In order to understand this difference, we numerically solve our kinetic equations with the

rates multiplied by a constant coefficients  $\kappa_a$  ( $a = 1, 2, 3, 4$ ) as follows.

$$\bar{\Gamma}_N \rightarrow \kappa_1 \bar{\Gamma}_N, \quad (9.5a)$$

$$\bar{\bar{\Gamma}}_N \rightarrow \kappa_2 \bar{\bar{\Gamma}}_N, \quad (9.5b)$$

$$\bar{\Gamma}_\nu \rightarrow \kappa_3 \bar{\Gamma}_\nu, \quad (9.5c)$$

$$\bar{\bar{\Gamma}}_\nu \rightarrow \kappa_4 \bar{\bar{\Gamma}}_\nu. \quad (9.5d)$$

Four different cases are considered.

**case 1** :  $\kappa_1 = \kappa_2 = \kappa_3 = \kappa_4 = 1$  for our equations (red lines in the following plot).

**case 2** :  $\kappa_1 = \kappa_2 = \kappa_3 = \kappa_4 = \frac{1}{2}$  for ref [23] by L. Canetti et al. (magenta lines).

**case 3** :  $\kappa_1 = \kappa_2 = 1$  and  $\kappa_3 = \kappa_4 = \frac{1}{2}$  for ref [32] M. Drewes et al. (blue lines).<sup>12</sup>

**case 4** :  $\kappa_1 = \kappa_4 = 1$  and  $\kappa_2 = \kappa_3 = \frac{1}{2}$  for ref [33] by P. Hernandez et al. (green lines).

For the cases 2, 3, and 4 the values above do not reproduce the kinetic equations in each works exactly, but allow us to understand the qualitative behaviour in each case.

We demonstrate the time-evolution of asymmetries up to  $T = 160$  GeV in figure 8. The

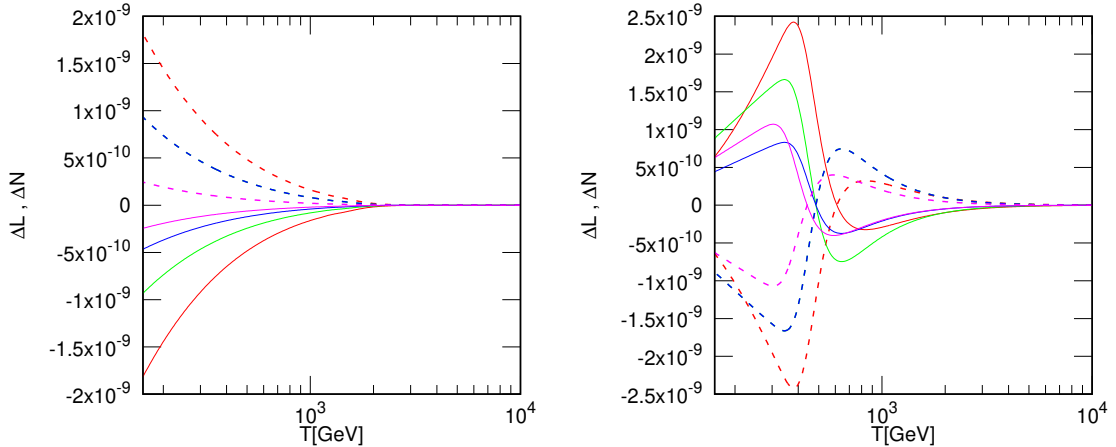


**Figure 8.** Time-evolution of asymmetries; solid lines are sum of asymmetries in the left-handed lepton sector and dashed lines are that of the HNL sector. Note that blue and green dashed lines are overlapped. The common mass  $M = 1$  GeV, phases are fixed to the values (8.1). *Left panel:*  $\Delta M = 10^{-7}$  GeV and  $\text{Im } \omega = 1$ . *Right panel:*  $\Delta M = 10^{-7}$  GeV and  $\text{Im } \omega = 5$ .

qualitative picture of figure 8 agrees with the results presented in figure 7.

There is also an important comment regarding studies of the parameter space. In fact, each point in this space defines a *theory*. It is not clear at all what could be a prior

<sup>12</sup> After the preprint of this paper had been released, we received a comment from the authors of refs. [32, 34]. They found a missing factor of two in their calculations. Once this factor is corrected, the relative sizes of the coefficients  $C_i$  in the corresponding row of table 2 will approximately agree with these of ref [33]. Namely, the **case 4** will be realized.

probability in the space of theories. The problem is not entirely philosophical. This can be most easily seen comparing the first columns of sub-plots in figures 4 and 5 from ref. [33] with the diagonal sub-plots in our figures 3 and 2. Our allowed regions of the parameters space are much larger than the contours shown in ref. [33]. The reason for this difference is that the study of ref. [33] relied on a Bayesian analysis of the Markov Chain Monte Carlo (MCMC). This analysis assumes certain prior probabilities in the space of theories and depends strongly on the chosen priors [33]. We advocate the point of view that each parameter point leading to the correct values of the observables (such as neutrino mixing angles and the value of the BAU) should be accounted for.

## 10 Conclusions and outlook

In this work we have performed the thorough study of the parameter space of baryogenesis in the  $\nu$ MSM. All important effects have been accounted for in our kinetic equations. Our study improves that of previous works in several respects.

(i) The rates entering kinetic equations are calculated from the parameters of the theory. In the symmetric phase, as one can see from the table 2, in ref. [23] the values of the rates were consistently underestimated. Moreover, apart from a factor of two difference in the damping rates, there is an agreement among all studies. Note also that all considered rates are practically the same in our work and in ref. [40].

(ii) In the broken phase the effects of the fermion number violation were systematically taken into account for the first time. These effects are important for the baryogenesis even though the temperature interval between the electroweak crossover and the sphaleron freeze-out is rather small.

(iii) We have accurately accounted for the sphaleron freeze-out utilizing the ‘improved approach’ of ref. [38].

(iv) Last but not the least improvement is related to the performance of the ODE solver which was used to solve the kinetic equations numerically. Impressive increase of efficiency of the numerical routine allowed us to perform a comprehensive sampling of the parameter space.

Our main results are upper and lower bounds of the region where successful baryogenesis in the  $\nu$ MSM is possible. We list them and stress significant points.

- Bounds in the  $|U|^2 - M$  plane, figure 1. The allowed region is significantly larger for light HNLs compared to the previous studies. Let us emphasize that the position of the upper bound is actually important for the direct detection. Even though this region seems to be the easiest for the direct detection owing to the most efficient production of HNLs, it might be actually not the case, because the life time of HNLs is short. HNLs can decay before they reach the detector. See the line of the SHiP experiment in figure 1. Also, it might be interesting to update the study of the neutrinoless double beta decay in the  $\nu$ MSM, refs. [30, 31, 33].

- Bounds on individual mixings  $|U_\alpha| \cdot |U_\beta|$  as functions of  $M$ . Note that we present also the off-diagonal elements. These are important for thorough simulations of the experimental sensitivity.
- The dataset of different choices of the parameters of the  $\nu$ MSM. This dataset can be used to compare our approach with other groups. As we have already stressed, we use momentum averaged kinetic equations. Computation of the BAU in the full system is highly non-trivial and a scan of the parameter space is very demanding. Therefore our parameter sets can be used as benchmark points to test different regimes of the BAU production with the accurate non-averaged equations. Models from the dataset could also be used by experimental collaborations for Monte Carlo simulations.

## Acknowledgments

We are grateful to Jacopo Ghiglieri and Mikko Laine for helpful discussions and for sharing the numerical data on the direct rates from ref. [69]. We thank Alexey Boyarsky, Jacopo Ghiglieri, Mikko Laine, and Oleg Ruchayskiy for helpful comments on the paper. We thank Juraj Claric for useful discussions and for sharing the data points from ref. [34]. We also thank Jacobo López-Pavón for discussions related to the plasma neutrality and the comparison of kinetic equations. This work was supported by the ERC-AdG-2015 grant 694896. The work of M.S. and I.T. was supported partially by the Swiss National Science Foundation.

## A Mixings of HNLs and active neutrinos

In this appendix we collect the formulae for the mixings of HNLs and active neutrinos. We considered the two-HNL case here. All formulae presented here are obtained for the normal hierarchy (NH) of the neutrino masses. The case of the inverted hierarchy (IH) can be obtained by the following replacement

$$\text{NH} \rightarrow \text{IH} : \quad m_2 \rightarrow m_1, \quad m_3 \rightarrow m_2, \quad U_{\alpha 2}^{PMNS} \rightarrow U_{\alpha 1}^{PMNS}, \quad U_{\alpha 3}^{PMNS} \rightarrow U_{\alpha 2}^{PMNS} \quad (\text{A.1})$$

So, for example,  $m_2 + m_3$  becomes  $m_1 + m_2$  in the IH case.

The Yukawa coupling constants entering the Lagrangian (2.1) can be decomposed using the Casas-Ibarra parametrization (2.4). Formula (2.4) can be rewritten as

$$F_{\alpha 1} = \frac{\sqrt{M_1}}{2\langle\Phi(0)\rangle} \left[ C_\alpha^+ \tilde{X}_\omega + C_\alpha^- \tilde{X}_\omega^{-1} \right], \quad (\text{A.2})$$

$$F_{\alpha 2} = i \frac{\sqrt{M_2}}{2\langle\Phi(0)\rangle} \left[ C_\alpha^+ \tilde{X}_\omega - C_\alpha^- \tilde{X}_\omega^{-1} \right], \quad (\text{A.3})$$

where

$$M_1 = M - \Delta M, \quad (\text{A.4})$$

$$M_2 = M + \Delta M, \quad (\text{A.5})$$

$$\tilde{X}_\omega = X_\omega e^{-i\text{Re}\omega}, \quad (\text{A.6})$$

$$C_\alpha^+ = iU_{\alpha 2}^{PMNS}\sqrt{m_2} + \xi U_{\alpha 3}^{PMNS}\sqrt{m_3}, \quad (\text{A.7})$$

$$C_\alpha^- = iU_{\alpha 2}^{PMNS}\sqrt{m_2} - \xi U_{\alpha 3}^{PMNS}\sqrt{m_3}, \quad (\text{A.8})$$

the Higgs vev at zero temperature is  $\langle\Phi(0)\rangle = 174.1$  GeV. In the case of two HNLs the PMNS matrix contains two phases:

$$U^{PMNS} = \begin{pmatrix} c_{12}c_{13} & s_{12}c_{13}e^{i\eta} & s_{13}e^{-i\delta} \\ -s_{12}c_{23} - c_{12}s_{13}s_{23}e^{i\delta} & (c_{12}c_{23} - s_{12}s_{13}s_{23}e^{i\delta})e^{i\eta} & c_{13}s_{23} \\ s_{12}s_{23} - c_{12}s_{13}c_{23}e^{i\delta} & -(c_{12}s_{23} + s_{12}s_{13}c_{23}e^{i\delta})e^{i\eta} & c_{13}c_{23} \end{pmatrix}. \quad (\text{A.9})$$

Up to the leading order of the seesaw mechanism the mixing elements of HNLs are

$$\Theta_{\alpha 1} = \frac{\langle\Phi(0)\rangle F_{\alpha 1}}{M_1} = \frac{1}{2\sqrt{M_1}} [C_\alpha^+ \tilde{X}_\omega + C_\alpha^- \tilde{X}_\omega^{-1}], \quad (\text{A.10})$$

$$\Theta_{\alpha 2} = \frac{\langle\Phi(0)\rangle F_{\alpha 2}}{M_2} = \frac{i}{2\sqrt{M_2}} [C_\alpha^+ \tilde{X}_\omega - C_\alpha^- \tilde{X}_\omega^{-1}]. \quad (\text{A.11})$$

It is possible to show that the flavour components of the mixings are given by

$$|U_\alpha|^2 = \sum_I |\Theta_{\alpha I}|^2 \quad (\text{A.12})$$

$$= \frac{1}{2(M^2 - \Delta M^2)} [M(|C_\alpha^+|^2 X_\omega^2 + |C_\alpha^-|^2 X_\omega^{-2}) + 2\Delta M \text{Re}[C_\alpha^+ (C_\alpha^-)^* e^{-i2\text{Re}\omega}]] \quad (\text{A.13})$$

$$\simeq \frac{1}{2M} \left[ (|C_\alpha^+|^2 X_\omega^2 + |C_\alpha^-|^2 X_\omega^{-2}) + 2\frac{\Delta M}{M} \text{Re}[C_\alpha^+ (C_\alpha^-)^* e^{-i2\text{Re}\omega}] \right] \quad (\text{A.14})$$

$$\simeq \frac{1}{2M} [|C_\alpha^+|^2 X_\omega^2 + |C_\alpha^-|^2 X_\omega^{-2}], \quad (\text{A.15})$$

where

$$|C_\alpha^+|^2 = |U_{\alpha 2}^{PMNS}|^2 m_2 + |U_{\alpha 3}^{PMNS}|^2 m_3 - 2\xi\sqrt{m_2 m_3} \text{Im}[U_{\alpha 2}^{PMNS} U_{\alpha 3}^{PMNS*}], \quad (\text{A.16})$$

$$|C_\alpha^-|^2 = |U_{\alpha 2}^{PMNS}|^2 m_2 + |U_{\alpha 3}^{PMNS}|^2 m_3 + 2\xi\sqrt{m_2 m_3} \text{Im}[U_{\alpha 2}^{PMNS} U_{\alpha 3}^{PMNS*}], \quad (\text{A.17})$$

$$\text{Re}[C_\alpha^+ (C_\alpha^-)^* e^{-i2\text{Re}\omega}] = (|U_{\alpha 2}|^2 m_2 - |U_{\alpha 3}^{PMNS}|^2 m_3) \cos(2\text{Re}\omega) - \quad (\text{A.18})$$

$$2\xi\sqrt{m_2 m_3} \text{Re}[U_{\alpha 2}^{PMNS} U_{\alpha 3}^{PMNS*}] \sin(2\text{Re}\omega). \quad (\text{A.19})$$

Using the unitarity of the PMNS matrix one can derive the following expression for the

total mixing

$$|U|^2 = \sum_{\alpha} |U_{\alpha}|^2 \quad (\text{A.20})$$

$$= \frac{1}{2(M^2 - \Delta M^2)} [M(m_2 + m_3)(X_{\omega}^2 + X_{\omega}^{-2}) + 2\Delta M(m_2 - m_3) \cos(\text{Re } \omega)] \quad (\text{A.21})$$

$$\simeq \frac{1}{2M} \left[ (m_3 + m_2)(X_{\omega}^2 + X_{\omega}^{-2}) - 2\frac{\Delta M}{M}(m_3 - m_2) \cos(\text{Re } \omega) \right] \quad (\text{A.22})$$

$$\simeq \frac{1}{2M} [(m_3 + m_2)(X_{\omega}^2 + X_{\omega}^{-2})]. \quad (\text{A.23})$$

Corresponding formulae in the IH case can be obtained by means of the replacement (A.1).

## B Derivation of the kinetic equations in Higgs phase

In this appendix we present the derivation of the kinetic equations in the Higgs phase. We consider only processes where the Higgs phase is substituted by its vev, i.e. only indirect processes (see, e.g. eq. (6.5)) which give the dominant contribution.

The kinetic equations accounting for the fermion number violating processes in the Higgs phase were derived in ref. [36]. A certain ansatz about the modification of the neutrino energies by the SM plasma has been made there. Here we extend the method of ref. [36] so that the interactions with the SM particles are consistently accounted for. This consideration is motivated by recent ref. [69] where an extra active neutrino rate, missing in the equations of ref. [36], is involved. Our derivation here confirms the results of ref. [69].

Below we derive the kinetic equations (6.1). First, we overview the idea behind the derivation and then present the actual calculations.

### B.1 Overview of the procedure

- The lepton asymmetry in the  $\nu$ MSM is generated due to interactions of active neutrinos with HNLs and coherent oscillations of the latter. Therefore we need to derive the equations describing the evolution of number densities of both active neutrinos,  $\rho_{\nu_{\alpha}}$  and HNLs  $\rho_{N_I}$  as well as correlations of HNLs.
- We work in the Heisenberg picture and introduce a time-independent density matrix of the complete system  $\boldsymbol{\rho}$ . The distribution function of a particle created by an operator  $a^{\dagger}$  is given then by  $\text{Tr}[a^{\dagger} a \boldsymbol{\rho}]$ .
- The time evolution of an operator  $\mathcal{O}$  is governed by the Heisenberg equation

$$\frac{d}{dt} \mathcal{O}(t) = i[H, \mathcal{O}(t)], \quad (\text{B.1})$$

where  $H$  is the Hamiltonian of the system. We are interested in the operators of the type  $\mathcal{O} = a^{\dagger} a$ . So we need to derive the Hamiltonian in terms of creation and annihilation operators.

- The evolution equations for the operators describing the number densities of neutrinos and HNLs and correlations of HNLs involve some new operators. We write down the evolution equations for these new operators. These equations, in turn, involve new operators. We keep going until the system of the equations closes (note that this is very different from the Bogolyubov-Born-Green-Kirkwood-Yvon hierarchy which should be truncation at some level).
- We obtain a set of a large number of first-order ordinary differential equations. Noticing that distinct time scales are present in these equations, one can integrate out fast oscillations and obtain a system describing the slow evolution of the quantities of interest (number densities and correlations).

## B.2 Lagrangian and Hamiltonian

The Lagrangian in the mass basis (2.1) is useful for a study of the phenomenology of the  $\nu$ MSM. For the derivation of the kinetic equations it is more convenient to change the basis [15] so the Lagrangian reads (we use tilde  $\tilde{N}_I$  to indicate the different basis)

$$\mathcal{L}_{\text{SM}+2\text{RH}\nu} = \mathcal{L}_0 + \Delta\mathcal{L}, \quad (\text{B.2a})$$

$$\mathcal{L}_0 = \mathcal{L}_{\text{SM}} + \overline{\tilde{N}_I} i \partial_\mu \gamma^\mu \tilde{N}_I - (h_{\alpha 2} \overline{L_\alpha} \tilde{N}_2 \tilde{\Phi} + M \overline{\tilde{N}_2^c} \tilde{N}_3 + h.c.), \quad (\text{B.2b})$$

$$\Delta\mathcal{L} = -h_{\alpha 3} \overline{L_\alpha} \tilde{N}_3 \tilde{\Phi} - \frac{\Delta M}{2} \overline{\tilde{N}_I^c} \tilde{N}_I + h.c., \quad (\text{B.2c})$$

where  $\Delta M$  is the Majorana mass difference so that the mass matrix of two heavier HNLs is  $M_I = \text{diag}(M - \Delta M, M + \Delta M)$ . The matrix of Yukawa couplings  $h_{\alpha I}$  can be related to the matrix  $F_{\alpha I}$  defined in (2.1) as follows

$$F_{\alpha I} = h_{\alpha J} [U_N^*]_{JI}, \quad (\text{B.3})$$

$$U_N = \frac{1}{\sqrt{2}} \begin{pmatrix} -i & 1 \\ i & 1 \end{pmatrix}. \quad (\text{B.4})$$

It is convenient to further rewrite the Lagrangian (B.2) by unifying two Majorana fields into one Dirac field  $\Psi = N_2^c + N_3$ . After that, the Lagrangian in the Higgs phase reads

$$\mathcal{L} = \mathcal{L}_{\text{SM}} + \overline{\Psi} i \partial_\mu \gamma^\mu \Psi - M \overline{\Psi} \Psi + \mathcal{L}_{\text{int}}, \quad (\text{B.5})$$

$$\mathcal{L}_{\text{int}} = -\frac{\Delta M}{2} (\overline{\Psi} \Psi^c + \overline{\Psi^c} \Psi) - (h_{\alpha 2} \langle \Phi \rangle \overline{\nu_{L\alpha}} \Psi + h_{\alpha 3} \langle \Phi \rangle \overline{\nu_{L\alpha}} \Psi^c + h.c.), \quad (\text{B.6})$$

where  $\mathcal{L}_{\text{SM}}$  is the SM part,  $M = (M_3 + M_2)/2$  and  $\Delta M = (M_3 - M_2)/2$  are the common mass and Majorana mass difference,  $\langle \Phi \rangle = \langle \Phi(T) \rangle$  is the temperature dependent Higgs vacuum expectation value,  $\langle \Phi(0) \rangle = 174.1$  GeV.

We treat the mass difference of HNLs and their interactions with left-handed neutrinos as small perturbations. It is important that all the SM interactions—including these of active neutrinos—occur with much larger rates compared to those originating from the (B.6). It is therefore reasonable to formulate a perturbation theory in small parameters of (B.6). In what follows we realize this program.

The momentum expansion of the HNLs field is given by

$$\Psi(x) = \int \frac{d^3\mathbf{p}}{(2\pi)^3 \sqrt{2E_p}} \sum_{s=\pm} \left( a_s(\mathbf{p}) u(p, s) e^{-ipx} + b_s^\dagger(\mathbf{p}) v(p, s) e^{ipx} \right). \quad (\text{B.7})$$

We orient  $\mathbf{p}$  along the  $z$  axis. choose plane wave solutions  $u(p, s)$  and  $v(p, s)$  the helicity states of  $\Psi$  are  $s = \pm$  and the operators  $a_s$  and  $b_s$  obey the usual anticommutation relations

$$\begin{aligned} \{a_h(\mathbf{p}), a_{h'}^\dagger(\mathbf{p}')\} &= (2\pi)^3 \delta_{hh'} \cdot \delta(\mathbf{p} - \mathbf{p}'), \\ \{b_h(\mathbf{p}), b_{h'}^\dagger(\mathbf{p}')\} &= (2\pi)^3 \delta_{hh'} \cdot \delta(\mathbf{p} - \mathbf{p}') \end{aligned} \quad (\text{B.8})$$

with all other anticommutators equal to zero. We also introduce operators  $a_{\nu_\alpha}^\dagger(\mathbf{p})$ ,  $a_{\nu_\alpha}(\mathbf{p})$ ,  $b_{\nu_\alpha}^\dagger(\mathbf{p})$  and  $b_{\nu_\alpha}(\mathbf{p})$  describing the SM neutrinos and antineutrinos correspondingly,  $\alpha = e, \mu, \tau$ . These operators obey analogous anticommutation relations.

In the HNL sector, we assign a positive fermion number to a particle with a positive helicity and to an antiparticle with a negative helicity. For instance, one HNL is created by  $a_+^\dagger(\pm\mathbf{p})$  and another one is created by  $b_-^\dagger(\pm\mathbf{p})$ , see table 3. Attributed in this way, the fermion number is conserved in the limit  $M \rightarrow 0, \Delta M \rightarrow 0$ .

	particles	antiparticles
HNLs	$a_+^\dagger(\pm\mathbf{p}), b_-^\dagger(+\mathbf{p})$	$a_-^\dagger(\pm\mathbf{p}), b_+^\dagger(+\mathbf{p})$
neutrinos	$a_{\nu_\alpha}^\dagger(\pm\mathbf{p})$	$b_{\nu_\alpha}^\dagger(\pm\mathbf{p})$

**Table 3.** Creation operators for particles and antiparticles.

We will work in the matrix of densities formalism inspired by ref. [87]. At the end of the day, we want to describe the distribution functions of HNLs and their coherent oscillations. Therefore we are interested in time evolution of bilinears of the type  $\mathcal{O} = a_N^\dagger(\mathbf{p}, +1) a_N(\mathbf{p}, +1)$ . The time evolution of such operators is governed by the Heisenberg equation

$$\frac{d}{dt} \mathcal{O}(t) = i[H, \mathcal{O}(t)], \quad (\text{B.9})$$

where  $H$  is the total Hamiltonian of the system. This Hamiltonian can be decomposed as

$$H = H_0 + H_{int} + H_{int}^{SM}. \quad (\text{B.10})$$

In the last expression,  $H_0$  is the Hamiltonian of the free Dirac field  $\Psi$  and the free Weyl fields  $\nu_{L_\alpha}$ ;  $H_{int}$  describes *quadratic* interactions of the HNLs and left-handed neutrinos and  $H_{int}^{SM}$  is the Hamiltonian describing all SM interactions of  $\nu_{L_\alpha}$ .

In order to be able to use eq. (B.9) we express the Hamiltonian (B.10) in terms of creation and annihilation operators. For the first and the second terms in eq (B.10) it is a tedious but straightforward task. The SM part has to be treated separately.



Using (B.7) and analogous decomposition for the neutrino fields, one can find that the free Hamiltonian  $H_0$  is given by

$$H_0 = \int \frac{d^3\mathbf{p}}{(2\pi)^3} \sum_{h=\pm 1} E_N(\mathbf{p}) \left( a_N^\dagger(\mathbf{p}, h) a_N(\mathbf{p}, h) + b_N^\dagger(\mathbf{p}, h) b_N(\mathbf{p}, h) \right) + \quad (\text{B.11})$$

$$\sum_{\alpha=e,\mu,\tau} \int \frac{d^3\mathbf{p}}{(2\pi)^3} E_{\nu_\alpha} \left( a_{\nu_\alpha}^\dagger(\mathbf{p}) a_{\nu_\alpha}(\mathbf{p}) + b_{\nu_\alpha}^\dagger(\mathbf{p}) b_{\nu_\alpha}(\mathbf{p}) \right), \quad (\text{B.12})$$

where  $E_N(\mathbf{p})$  and  $E_{\nu_\alpha}(\mathbf{p})$  are the energies of HNLs and active neutrinos. As the SM model effects are accounted for, the energy of the active neutrino must be replaced by a temperature dependent dispersion relation, see e.g. refs [74, 75]. We will use the same symbol  $E_{\nu_\alpha}$  for both vacuum and thermal energies of neutrinos. Note, however, that  $E_{\nu_\alpha}$  in medium can deviate significantly from the vacuum value which is just  $|\mathbf{p}|$  (the small neutrino masses can be safely neglected).

The interaction Hamiltonian  $H_{int}$  can be further decomposed into the Majorana and Yukawa parts coming from the first and the second parenthesis in (B.6) respectively

$$H_{int} = H_{int}^{Majorana} + H_{int}^Y. \quad (\text{B.13})$$

The Majorana part of the interaction Hamiltonian is

$$H_{int}^{Majorana} = \int \frac{d^3\mathbf{p}}{(2\pi)^3} \mathcal{H}^M, \quad (\text{B.14})$$

$$\begin{aligned} \mathcal{H}^M = & \frac{p\Delta M}{E_N} \left( a_-(\mathbf{p}) a_-(-\mathbf{p}) + a_+(\mathbf{p}) a_+(-\mathbf{p}) + b_+^\dagger(\mathbf{p}) b_+^\dagger(-\mathbf{p}) + b_-^\dagger(\mathbf{p}) b_-^\dagger(-\mathbf{p}) \right) + \\ & \frac{M\Delta M}{E_N} \left( b_+(\mathbf{p}) a_-^\dagger(\mathbf{p}) + b_-(-\mathbf{p}) a_+^\dagger(-\mathbf{p}) + a_+^\dagger(\mathbf{p}) b_-(\mathbf{p}) + a_-^\dagger(-\mathbf{p}) b_+(\mathbf{p}) \right) + \\ & \frac{p\Delta M}{E_N} \left( b_+(-\mathbf{p}) b_+(\mathbf{p}) + b_-(-\mathbf{p}) b_-(\mathbf{p}) + a_-^\dagger(-\mathbf{p}) a_-^\dagger(\mathbf{p}) + a_+^\dagger(-\mathbf{p}) a_+^\dagger(\mathbf{p}) \right) + \\ & \frac{M\Delta M}{E_N} \left( a_-(\mathbf{p}) b_+^\dagger(\mathbf{p}) + a_+(-\mathbf{p}) b_-^\dagger(-\mathbf{p}) + b_-^\dagger(\mathbf{p}) a_+(\mathbf{p}) + b_+^\dagger(-\mathbf{p}) a_-(-\mathbf{p}) \right), \end{aligned} \quad (\text{B.15})$$

where  $p \equiv |\mathbf{p}|$ .

The part of the interaction Hamiltonian coming from the Yukawa interactions reads

$$\begin{aligned}
H_{int}^Y &= \sum_{\alpha=e,\mu,\tau} \int \frac{d^3\mathbf{p}}{(2\pi)^3} \mathcal{H}^Y \quad (\text{B.16}) \\
\mathcal{H}^Y &= h_{\alpha 2}^* K(\mathbf{p}) \left( -b_{-}(\mathbf{p}) b_{\nu_{\alpha}}^{\dagger}(\mathbf{p}) - b_{-}(-\mathbf{p}) b_{\nu_{\alpha}}^{\dagger}(-\mathbf{p}) + a_{-}^{\dagger}(\mathbf{p}) a_{\nu_{\alpha}}(\mathbf{p}) + a_{-}^{\dagger}(-\mathbf{p}) a_{\nu_{\alpha}}(-\mathbf{p}) \right) + \\
&\quad h_{\alpha 2} K(\mathbf{p}) \left( -b_{\nu_{\alpha}}(\mathbf{p}) b_{-}^{\dagger}(\mathbf{p}) - b_{\nu_{\alpha}}(-\mathbf{p}) b_{-}^{\dagger}(-\mathbf{p}) + a_{\nu_{\alpha}}^{\dagger}(\mathbf{p}) a_{-}(\mathbf{p}) + a_{\nu_{\alpha}}^{\dagger}(-\mathbf{p}) a_{-}(-\mathbf{p}) \right) - \\
&\quad h_{\alpha 3}^* K(\mathbf{p}) \left( a_{+}(\mathbf{p}) b_{\nu_{\alpha}}^{\dagger}(\mathbf{p}) - a_{+}(-\mathbf{p}) b_{\nu_{\alpha}}^{\dagger}(-\mathbf{p}) + b_{+}^{\dagger}(\mathbf{p}) a_{\nu_{\alpha}}(\mathbf{p}) - b_{+}^{\dagger}(-\mathbf{p}) a_{\nu_{\alpha}}(-\mathbf{p}) \right) - \\
&\quad h_{\alpha 3} K(\mathbf{p}) \left( b_{\nu_{\alpha}}(\mathbf{p}) a_{+}^{\dagger}(\mathbf{p}) - b_{\nu_{\alpha}}(-\mathbf{p}) a_{+}^{\dagger}(-\mathbf{p}) + a_{\nu_{\alpha}}^{\dagger}(\mathbf{p}) b_{+}(\mathbf{p}) - a_{\nu_{\alpha}}^{\dagger}(-\mathbf{p}) b_{+}(-\mathbf{p}) \right) - \\
&\quad h_{\alpha 2}^* \tilde{K}(\mathbf{p}) \left( b_{+}(\mathbf{p}) a_{\nu_{\alpha}}(-\mathbf{p}) + b_{+}(-\mathbf{p}) a_{\nu_{\alpha}}(\mathbf{p}) - a_{+}^{\dagger}(\mathbf{p}) b_{\nu_{\alpha}}^{\dagger}(-\mathbf{p}) - a_{+}^{\dagger}(-\mathbf{p}) b_{\nu_{\alpha}}^{\dagger}(\mathbf{p}) \right) - \\
&\quad h_{\alpha 2} \tilde{K}(\mathbf{p}) \left( -b_{\nu_{\alpha}}(\mathbf{p}) a_{+}(-\mathbf{p}) - b_{\nu_{\alpha}}(-\mathbf{p}) a_{+}(\mathbf{p}) + a_{\nu_{\alpha}}^{\dagger}(\mathbf{p}) b_{+}^{\dagger}(-\mathbf{p}) + a_{\nu_{\alpha}}^{\dagger}(-\mathbf{p}) b_{+}^{\dagger}(\mathbf{p}) \right) - \\
&\quad h_{\alpha 3}^* \tilde{K}(\mathbf{p}) \left( -a_{-}(\mathbf{p}) a_{\nu_{\alpha}}(-\mathbf{p}) + a_{-}(-\mathbf{p}) a_{\nu_{\alpha}}(\mathbf{p}) - b_{-}^{\dagger}(\mathbf{p}) b_{\nu_{\alpha}}^{\dagger}(-\mathbf{p}) + b_{-}^{\dagger}(-\mathbf{p}) b_{\nu_{\alpha}}^{\dagger}(\mathbf{p}) \right) - \\
&\quad h_{\alpha 3} \tilde{K}(\mathbf{p}) \left( b_{\nu_{\alpha}}(\mathbf{p}) b_{-}(-\mathbf{p}) - b_{\nu_{\alpha}}(-\mathbf{p}) b_{-}(\mathbf{p}) + a_{\nu_{\alpha}}^{\dagger}(\mathbf{p}) a_{-}^{\dagger}(-\mathbf{p}) - a_{\nu_{\alpha}}^{\dagger}(-\mathbf{p}) a_{-}^{\dagger}(\mathbf{p}) \right), \quad (\text{B.17})
\end{aligned}$$

where

$$K(\mathbf{p}) = \frac{\langle \Phi \rangle \sqrt{E_{\nu}(E_N - p)}}{\sqrt{2E_N E_{\nu}}}, \quad \tilde{K}(\mathbf{p}) = \frac{\langle \Phi \rangle \sqrt{E_{\nu}(E_N + p)}}{\sqrt{2E_N E_{\nu}}}. \quad (\text{B.18})$$

The interactions of active neutrinos with the SM plasma are described by the following Hamiltonian.

$$H_{int}^{SM} = \int d^3x G_F \left( \bar{\nu}_{L\alpha} J + J^{\dagger} \nu_{L\alpha} \right), \quad (\text{B.19})$$

where  $J$  is the SM current coupled to neutrino. It is important that  $J$  anticommutes with the creation and annihilation operators from table 3.

### B.3 Commutators and averaging

Now we can use the Hamiltonian (B.10) to derive the evolution equations. However, first we need to identify the operators of interest.

Note that the interaction Hamiltonians (B.14) and (B.16) contain both positive and negative  $\mathbf{p}$ . The distribution functions of HNLs and active neutrino can be constructed from the operators

$$\begin{aligned}
&a_{+}^{\dagger}(+\mathbf{p}) a_{+}(+\mathbf{p}), \quad a_{+}^{\dagger}(+\mathbf{p}) b_{-}(+\mathbf{p}), \quad b_{-}^{\dagger}(+\mathbf{p}) a_{+}(+\mathbf{p}), \quad b_{-}^{\dagger}(+\mathbf{p}) b_{-}(+\mathbf{p}), \\
&a_{\nu_{\alpha}}^{\dagger}(+\mathbf{p}) a_{\nu_{\alpha}}(+\mathbf{p}), \quad (\text{B.20})
\end{aligned}$$

or from the operators with inverted sign of the spatial momentum

$$\begin{aligned}
&a_{+}^{\dagger}(-\mathbf{p}) a_{+}(-\mathbf{p}), \quad a_{+}^{\dagger}(-\mathbf{p}) b_{-}(-\mathbf{p}), \quad b_{-}^{\dagger}(-\mathbf{p}) a_{+}(-\mathbf{p}), \quad b_{-}^{\dagger}(-\mathbf{p}) b_{-}(-\mathbf{p}), \\
&a_{\nu_{\alpha}}^{\dagger}(-\mathbf{p}) a_{\nu_{\alpha}}(-\mathbf{p}). \quad (\text{B.21})
\end{aligned}$$

Operators (B.20) and (B.21) will be mixed after commuting them with the interaction Hamiltonians. Nevertheless, this apparent duplication is not a problem. Notice that operators (B.21) can be obtained from (B.20) by a parity transformation. Combining operators (B.20) with those obtained by a parity transformation one can define

$$\begin{aligned}
\mathcal{O}_{11} &= a_+^\dagger(+\mathbf{p})a_+(+\mathbf{p}) + a_+^\dagger(-\mathbf{p})a_+(-\mathbf{p}), \\
\mathcal{O}_{12} &= a_+^\dagger(+\mathbf{p})b_-(+\mathbf{p}) - a_+^\dagger(-\mathbf{p})b_-(-\mathbf{p}), \\
\mathcal{O}_{21} &= b_-^\dagger(+\mathbf{p})a_+(+\mathbf{p}) - b_-^\dagger(-\mathbf{p})a_+(-\mathbf{p}), \\
\mathcal{O}_{22} &= b_-^\dagger(+\mathbf{p})b_-(+\mathbf{p}) + b_-^\dagger(-\mathbf{p})b_-(-\mathbf{p}), \\
\mathcal{O}_{\nu_\alpha} &= a_{\nu_\alpha}^\dagger(+\mathbf{p})a_{\nu_\alpha}(+\mathbf{p}) + a_{\nu_\alpha}^\dagger(-\mathbf{p})a_{\nu_\alpha}(-\mathbf{p}), \quad \alpha = e, \mu, \tau,
\end{aligned} \tag{B.22}$$

where the minus signs in (B.22) appear as a consequence of the negative intrinsic parity of  $b_\pm$  in our representation. The operators describing the antiparticles are constructed in full analogy with (B.22) using the definitions in table 3.

Now we commute the operators (B.22) with the full Hamiltonian (B.10) in order to write down the evolution equations (B.9). Let us illustrate the procedure considering the operator  $a_+^\dagger(+\mathbf{p})a_+(+\mathbf{p})$  only. The Heisenberg equation for this operator reads

$$-i\frac{d}{dt}\left(a_+^\dagger(\mathbf{p})a_+(\mathbf{p})\right) = \left[H, a_+^\dagger(\mathbf{p})a_+(\mathbf{p})\right] = h_{e2}K(\mathbf{p})a_{\nu_e}^\dagger(\mathbf{p})a_+^\dagger(\mathbf{p}) + \dots \tag{B.23}$$

The commutator contains 16 different operators, most of them are other than (B.20) and (B.21). We have explicitly shown only one new operator, let us denote it  $\mathcal{O}_1^{fast} \equiv a_{\nu_e}^\dagger(\mathbf{p})a_+^\dagger(\mathbf{p})$ . It is important that all terms on the r.h.s. of (B.23) are proportional to small parameters, either Yukawa couplings or Majorana mass difference. Now we need the Heisenberg equation for  $\mathcal{O}_1^{fast}$ , which is

$$-i\frac{d}{dt}\mathcal{O}_1^{fast} = \left[H, \mathcal{O}_1^{fast}\right] = (E_{\nu_e} - E_N)\mathcal{O}_1^{fast} + \sum_k C_k \mathcal{O}_k^{fast} + \sum_l C_l' \mathcal{O}_l^{slow} + \sum_l C_m'' \mathcal{O}_m^{medium}, \tag{B.24}$$

where the first term on r.h.s. arises due to the commutation of  $\mathcal{O}_1^{fast}$  with  $H_0$ , the terms  $\mathcal{O}_k^{fast}$  and  $\mathcal{O}_l^{slow}$  come from the commutation with  $H_{int}$  and operators  $\mathcal{O}_m^{medium}$  come from the commutation with  $H_{int}^{SM}$ .

Note the difference between (B.23) and (B.24): the time derivative of  $a_+^\dagger(\mathbf{p})a_+(\mathbf{p})$  is proportional to the small parameter  $h_{e2}$ , whereas the time derivative  $\mathcal{O}_1^{fast}$  is proportional to  $i(E_{\nu_e} - E_N)\mathcal{O}_1^{fast}$ . In what follows we will call “slow” the operators whose time derivatives are proportional to the small parameters, such as Yukawas. All other operators are “fast”. All operators (B.22) (as well as (B.20) and (B.21) separately) do commute with the free Hamiltonian (B.12) and therefore they are of the slow type. The operators  $\mathcal{O}_k^{fast}$  present in the commutators of (B.22) with the full Hamiltonian are of the fast type.

We derive equations analogous to (B.24) for all operators appearing in the commutators of the operators (B.22) with  $H$ . These equations would form a closed set if not the SM interactions. Indeed, there are no equations for terms  $C_m'' \mathcal{O}_m^{medium}$ . These terms have the form, e.g.,  $\bar{u}_\nu(-\mathbf{p}, h)a_h(\mathbf{p})J(b\mathbf{p})$ , where  $J(\mathbf{p})$  is the Fourier transform of the medium current

$J(x)$ . We now derive the evolution equation for  $\mathcal{O}_m^{medium}$ . It has the following form.

$$-i \frac{d}{dt} \mathcal{O}_m^{medium} = [H, \mathcal{O}_m^{medium}] = E_N \mathcal{O}_m^{medium} + C''' \mathcal{O}_k^{fast} + \dots, \quad (\text{B.25})$$

where dots denote other fast operators which are already present in our system. Equations of type (B.23), (B.24) and (B.25) now form the closed system. This system can be schematically written as

$$i \dot{x}_i = \sum_j (\epsilon a_{ij} x_j + \epsilon b_{ij} y_j), \quad (\text{B.26a})$$

$$i \dot{y}_k = -E_k y_k + \sum_l (\epsilon c_{kl} x_l + \epsilon d_{kl} y_l), \quad (\text{B.26b})$$

where  $x_i$  are the slow operators (B.22) (their derivatives are proportional to small parameter  $\epsilon$ ), while variables  $y_k$  are fast. All coefficients  $a, b, c, d$  are time dependent functions of order of unity and  $E_k$  are combinations of energies of HNLs and active neutrinos of type  $E_N + E_{\nu_\alpha}$ ,  $E_{\nu_\alpha} - E_{\nu_\beta}$ , etc. Note that there is no summation over  $k$  in (B.26b). For the sake of clarity we have assumed the following power counting, both Majorana mass differences and Yukawas times the Higgs vacuum expectation value are proportional to a small dimensional parameter  $\Delta M, h \cdot \langle \Phi \rangle \propto \epsilon$ .

We will show now, that the fast oscillations can be averaged or—in the language of effective theories—integrated out in the way that the final system describes the slow evolution of operators.

Let us first consider the system at moment  $\bar{t}$ . With the fixed  $x_i(\bar{t}) = \bar{x}_i$  eqs (B.26b) read

$$i \dot{y}_k = -E_k y_k + \sum_l (\epsilon c_{kl} \bar{x}_l + \epsilon d_{kl} y_l). \quad (\text{B.27})$$

We choose a time interval  $t \in [\bar{t}, \bar{t} + T]$ , such that  $1/E \ll T \ll 1/\epsilon$ , where  $E$  is of order of  $E_N$  or  $E_{\nu_\alpha}$ . The first inequality means that  $x_i(t)$  does not change significantly on this time interval. We solve the system (B.27) on this interval and denoted the solution as  $\tilde{y}_k(t, \bar{x})$ . The second inequality allows us to exclude the fast oscillations from  $\tilde{y}_k(t, \bar{x})$  by means of the averaging

$$\bar{y}_k(\bar{t}, \bar{x}) = \frac{1}{T} \int_{\bar{t}}^{\bar{t}+T} dt \tilde{y}_k(t, \bar{x}). \quad (\text{B.28})$$

One can show that for the system (B.26) originating from the commutation of (B.22) with the full Hamiltonian (B.10), averaging (B.28) gives

$$\bar{y}_k(\bar{t}, \bar{x}) = \sum_l \frac{\epsilon c_{kl} \bar{x}_l}{E_k}. \quad (\text{B.29})$$

In practice, we first integrate out the interactions with medium. This allows us to express the operators  $\mathcal{O}_m^{medium}$  in the r.h.s. of (B.24) in terms of  $\mathcal{O}_k^{fast}$ . We are working in the leading order in small parameters  $\epsilon$ , as a result, it is only the first term in the r.h.s. of

(B.24) which should be modified. This modification can be summarized as

$$\begin{aligned} E_\nu - E_N &\rightarrow E_\nu - E_N - \frac{1}{k} \bar{u}_h(k) \not{\Sigma}(k) u_h(k), \\ E_\nu + E_N &\rightarrow E_\nu + E_N - \frac{1}{k} \bar{u}_h(-k) \not{\Sigma}(k) u_h(-k), \end{aligned} \quad (\text{B.30})$$

where  $\Sigma(k)$  is the active neutrino self energy and we have suppressed the flavour indices of the active neutrinos. The imaginary part of the self energy can be parametrized as [70]

$$\text{Im } \not{\Sigma}(k) = \not{k} \Gamma_k / 2 + \not{u} \Gamma_u / 2, \quad (\text{B.31})$$

where  $u^\mu = (1, 0, 0, 0)$  is the four-velocity of the medium.

Once the fast operators related to the medium are integrated out, we also get rid of the fast operators of the type  $\mathcal{O}_k^{fast}$ . Eventually one gets the closed set of equations in terms of the slow variables only. These equations have the following generic form

$$i \dot{\bar{x}}_i(\bar{t}) = \sum_j \epsilon a_{ij} \bar{x}_j + \sum_{j,l} \frac{\epsilon^2 b_{ij} c'_{j,l}}{E_\nu + E_N - i(\Gamma_u + 2k^0 \Gamma_k)} \bar{x}_j + \sum_{j,l} \frac{\epsilon^2 b_{ij} c''_{j,l}}{E_\nu - E_N - i\Gamma_u} \bar{x}_j, \quad (\text{B.32})$$

where we have separated the coefficients  $c_{j,l}$  into two groups,  $c'$  and  $c''$ . Eventually, the terms with  $c''$  and  $c'$  will lead to processes with and without fermion number violation correspondingly, see eq. (6.5).

#### B.4 The final form of the equations

In order to obtain the system of kinetic equations in the matrix form we introduce the convenient notations of ref. [36],

$$\begin{aligned} \rho_{\nu_\alpha} &= \text{Tr}[a_{\nu_\alpha}^\dagger(k) a_{\nu_\alpha}(k) \rho], \\ \rho_{\bar{\nu}_\alpha} &= \text{Tr}[b_{\nu_\alpha}^\dagger(k) b_{\nu_\alpha}(k) \rho], \end{aligned} \quad (\text{B.33})$$

$$\rho_N = \begin{pmatrix} \text{Tr}[a_+^\dagger(k) a_+(k) \rho] & \text{Tr}[a_+^\dagger(k) b_-(k) \rho] \\ \text{Tr}[b_-^\dagger(k) a_+(k) \rho] & \text{Tr}[b_-^\dagger(k) b_-(k) \rho] \end{pmatrix}, \quad (\text{B.34})$$

$$\rho_{\bar{N}} = \begin{pmatrix} \text{Tr}[a_-^\dagger(k) a_-(k) \rho] & \text{Tr}[a_-^\dagger(k) b_+(k) \rho] \\ \text{Tr}[b_+^\dagger(k) a_-(k) \rho] & \text{Tr}[b_+^\dagger(k) b_+(k) \rho] \end{pmatrix}. \quad (\text{B.35})$$

Using these notations we arrive at the following kinetic equations

$$i \frac{d\rho_{\nu_\alpha}}{dt} = -i \Gamma_{\nu_\alpha} \rho_{\nu_\alpha} + i \text{Tr}[\tilde{\Gamma}_{\nu_\alpha} \rho_{\bar{N}}], \quad (\text{B.36a})$$

$$i \frac{d\rho_{\bar{\nu}_\alpha}}{dt} = -i \Gamma_{\nu_\alpha}^* \rho_{\bar{\nu}_\alpha} + i \text{Tr}[\tilde{\Gamma}_{\nu_\alpha}^* \rho_N], \quad (\text{B.36b})$$

$$i \frac{d\rho_N}{dt} = [H_N, \rho_N] - \frac{i}{2} \{\Gamma_N, \rho_N\} + i \sum_\alpha \tilde{\Gamma}_N^\alpha \rho_{\bar{\nu}_\alpha}, \quad (\text{B.36c})$$

$$i \frac{d\rho_{\bar{N}}}{dt} = [H_N^*, \rho_{\bar{N}}] - \frac{i}{2} \{\Gamma_N^*, \rho_{\bar{N}}\} + i \sum_\alpha (\tilde{\Gamma}_N^\alpha)^* \rho_{\nu_\alpha}. \quad (\text{B.36d})$$

Expressions for the rates and the effective Hamiltonian are present in section 6 so we do not repeat them here.

Notice that  $\rho_N$ ,  $\rho_{\bar{N}}$ ,  $\rho_{\nu_\alpha}$  and  $\rho_{\bar{\nu}_\alpha}$  in eqs. (B.36) depend on momentum so there is fact a set of equations for each momentum mode. During the whole period of the asymmetry generation, the leptons are in thermal equilibrium and different momentum modes communicate to each other. Therefore, the appropriate variables for the r.h.s. of equations (B.36) are the chemical potentials. Subtracting (B.36b) from (B.36a) and introducing the Fermi-Dirac distribution function for massless neutrino  $f_\nu = 1/(e^{k/T} + 1)$  we can rewrite (in the limit of small chemical potentials) equations (B.36) in the following form [38]

$$i \frac{dn_{\Delta_\alpha}}{dt} = -2i \frac{\mu_\alpha}{T} \int \frac{d^3k}{(2\pi)^3} \Gamma_{\nu_\alpha} f_\nu (1 - f_\nu) + i \int \frac{d^3k}{(2\pi)^3} \left( \text{Tr}[\tilde{\Gamma}_{\nu_\alpha} \rho_{\bar{N}}] - \text{Tr}[\tilde{\Gamma}_{\nu_\alpha}^* \rho_N] \right), \quad (\text{B.37a})$$

$$i \frac{d\rho_N}{dt} = [H_N, \rho_N] - \frac{i}{2} \{ \Gamma_N, \rho_N - \rho_N^{eq} \} - \frac{i}{2} \sum_\alpha \tilde{\Gamma}_N^\alpha \left[ 2 \frac{\mu_\alpha}{T} f_\nu (1 - f_\nu) \right], \quad (\text{B.37b})$$

$$i \frac{d\rho_{\bar{N}}}{dt} = [H_N^*, \rho_{\bar{N}}] - \frac{i}{2} \{ \Gamma_N^*, \rho_{\bar{N}} - \rho_N^{eq} \} + \frac{i}{2} \sum_\alpha (\tilde{\Gamma}_N^\alpha)^* \left[ 2 \frac{\mu_\alpha}{T} f_\nu (1 - f_\nu) \right], \quad (\text{B.37c})$$

where  $\rho_N^{eq}$  is the equilibrium distribution function of HNLs.<sup>13</sup> Note that the r.h.s. of eq. (B.37a) is written in terms of the density of the  $\Delta_\alpha = L_\alpha - B/3$ , where  $L_\alpha$  are the lepton numbers and  $B$  is the total baryon number. These combinations are not affected by the fast sphaleron processes and changes only due to interactions with HNLs, therefore their derivatives are equal to the derivatives of the lepton number densities  $n_{L_\alpha}$ .

## C Rates in the symmetric phase

In this section we describe how the rates entering eqs. (B.37) are defined. For completeness we also include the fermion number violating Higgs decays and inverse decays in the symmetric phase.

## D Benchmark points

In this chapter we present several parameter sets along with the corresponding values of the  $Y_B$ . These sets can be used to compare the numerical results among different groups. The full datasets could be downloaded from [68]. Note that we use the latest global fit to neutrino data [88].

## References

- [1] P. Minkowski,  $\mu \rightarrow e\gamma$  at a Rate of One Out of  $10^9$  Muon Decays?, *Phys. Lett.* **67B** (1977) 421–428.
- [2] M. Gell-Mann, P. Ramond and R. Slansky, *Complex Spinors and Unified Theories*, *Conf. Proc.* **C790927** (1979) 315–321, [[1306.4669](#)].

---

<sup>13</sup>The equilibrium distribution function appears as a result of application of the detailed balance principle.

$M$ , GeV	$\Delta M$ , GeV	$\text{Im } \omega$	$\text{Re } \omega/\pi$	$\delta/\pi$	$\eta/\pi$
5.0000e-01	5.9794e-09	5.3897e+00	6.4803e-01	1.8599e+00	3.5291e-01
1.0000e+00	5.3782e-09	5.2607e+00	8.3214e-01	1.2708e+00	1.7938e+00
2.0000e+00	3.0437e-09	5.5435e+00	1.6514e+00	1.6384e+00	7.5733e-01
5.0000e+00	1.7945e-09	5.229e+00	1.7753e+00	1.4481e+00	1.2070e+00
1.0000e+01	2.7660e-09	4.4442e+00	8.4146e-01	1.7963e+00	9.2261e-01

**Table 4.** Parameter sets leading to the observed value of the BAU, NH case.

$M$ , GeV	$\Delta M$ , GeV	$\text{Im } \omega$	$\text{Re } \omega/\pi$	$\delta/\pi$	$\eta/\pi$
5.0000e-01	6.0739e-09	5.3788e+00	1.6652e+00	1.8721e+00	1.5305e+00
1.0000e+00	8.3058e-09	4.9049e+00	9.1389e-02	1.5365e+00	4.7998e-01
2.0000e+00	4.9537e-09	4.6975e+00	5.4153e-01	1.5263e+00	1.7442e+00
5.0000e+00	2.3906e-09	4.1620e+00	2.7838e-01	1.2930e+00	9.9034e-01
1.0000e+01	2.7097e-08	-4.2412e-01	2.5429e-01	1.6901e+00	1.6839e-01

**Table 5.** Parameter sets leading to the observed value of the BAU, IH case.

- [3] R. N. Mohapatra and G. Senjanovic, *Neutrino Mass and Spontaneous Parity Nonconservation*, *Phys. Rev. Lett.* **44** (1980) 912.
- [4] T. Yanagida, *Horizontal Symmetry and Masses of Neutrinos*, *Prog. Theor. Phys.* **64** (1980) 1103.
- [5] J. Schechter and J. W. F. Valle, *Neutrino Masses in  $SU(2) \times U(1)$  Theories*, *Phys. Rev.* **D22** (1980) 2227.
- [6] J. Schechter and J. W. F. Valle, *Neutrino Decay and Spontaneous Violation of Lepton Number*, *Phys. Rev.* **D25** (1982) 774.
- [7] T. Asaka, S. Blanchet and M. Shaposhnikov, *The nuMSM, dark matter and neutrino masses*, *Phys. Lett.* **B631** (2005) 151–156, [[hep-ph/0503065](#)].
- [8] T. Asaka and M. Shaposhnikov, *The nuMSM, dark matter and baryon asymmetry of the universe*, *Phys. Lett.* **B620** (2005) 17–26, [[hep-ph/0505013](#)].
- [9] S. Dodelson and L. M. Widrow, *Sterile-neutrinos as dark matter*, *Phys. Rev. Lett.* **72** (1994) 17–20, [[hep-ph/9303287](#)].
- [10] X.-D. Shi and G. M. Fuller, *A New dark matter candidate: Nonthermal sterile neutrinos*, *Phys. Rev. Lett.* **82** (1999) 2832–2835, [[astro-ph/9810076](#)].
- [11] A. D. Dolgov and S. H. Hansen, *Massive sterile neutrinos as warm dark matter*, *Astropart. Phys.* **16** (2002) 339–344, [[hep-ph/0009083](#)].
- [12] K. Abazajian, G. M. Fuller and M. Patel, *Sterile neutrino hot, warm, and cold dark matter*, *Phys. Rev.* **D64** (2001) 023501, [[astro-ph/0101524](#)].
- [13] E. K. Akhmedov, V. A. Rubakov and A. Yu. Smirnov, *Baryogenesis via neutrino oscillations*, *Phys. Rev. Lett.* **81** (1998) 1359–1362, [[hep-ph/9803255](#)].

- [14] M. Shaposhnikov, *A Possible symmetry of the nuMSM*, *Nucl. Phys.* **B763** (2007) 49–59, [[hep-ph/0605047](#)].
- [15] M. Shaposhnikov, *The nuMSM, leptonic asymmetries, and properties of singlet fermions*, *JHEP* **08** (2008) 008, [[0804.4542](#)].
- [16] L. Canetti and M. Shaposhnikov, *Baryon Asymmetry of the Universe in the NuMSM*, *JCAP* **1009** (2010) 001, [[1006.0133](#)].
- [17] T. Asaka and H. Ishida, *Flavour Mixing of Neutrinos and Baryon Asymmetry of the Universe*, *Phys. Lett.* **B692** (2010) 105–113, [[1004.5491](#)].
- [18] A. Anisimov, D. Besak and D. Bodeker, *Thermal production of relativistic Majorana neutrinos: Strong enhancement by multiple soft scattering*, *JCAP* **1103** (2011) 042, [[1012.3784](#)].
- [19] T. Asaka, S. Eijima and H. Ishida, *Kinetic Equations for Baryogenesis via Sterile Neutrino Oscillation*, *JCAP* **1202** (2012) 021, [[1112.5565](#)].
- [20] D. Besak and D. Bodeker, *Thermal production of ultrarelativistic right-handed neutrinos: Complete leading-order results*, *JCAP* **1203** (2012) 029, [[1202.1288](#)].
- [21] L. Canetti, M. Drewes and M. Shaposhnikov, *Sterile Neutrinos as the Origin of Dark and Baryonic Matter*, *Phys. Rev. Lett.* **110** (2013) 061801, [[1204.3902](#)].
- [22] M. Drewes and B. Garbrecht, *Leptogenesis from a GeV Seesaw without Mass Degeneracy*, *JHEP* **03** (2013) 096, [[1206.5537](#)].
- [23] L. Canetti, M. Drewes, T. Frossard and M. Shaposhnikov, *Dark Matter, Baryogenesis and Neutrino Oscillations from Right Handed Neutrinos*, *Phys. Rev.* **D87** (2013) 093006, [[1208.4607](#)].
- [24] B. Shuve and I. Yavin, *Baryogenesis through Neutrino Oscillations: A Unified Perspective*, *Phys. Rev.* **D89** (2014) 075014, [[1401.2459](#)].
- [25] D. Bodeker and M. Laine, *Kubo relations and radiative corrections for lepton number washout*, *JCAP* **1405** (2014) 041, [[1403.2755](#)].
- [26] A. Abada, G. Arcadi, V. Domcke and M. Lucente, *Lepton number violation as a key to low-scale leptogenesis*, *JCAP* **1511** (2015) 041, [[1507.06215](#)].
- [27] P. Hernández, M. Kekic, J. López-Pavón, J. Racker and N. Rius, *Leptogenesis in GeV scale seesaw models*, *JHEP* **10** (2015) 067, [[1508.03676](#)].
- [28] J. Ghiglieri and M. Laine, *Neutrino dynamics below the electroweak crossover*, *JCAP* **1607** (2016) 015, [[1605.07720](#)].
- [29] T. Hambye and D. Teresi, *Higgs doublet decay as the origin of the baryon asymmetry*, *Phys. Rev. Lett.* **117** (2016) 091801, [[1606.00017](#)].
- [30] M. Drewes and S. Eijima, *Neutrinoless double  $\beta$  decay and low scale leptogenesis*, *Phys. Lett.* **B763** (2016) 72–79, [[1606.06221](#)].
- [31] T. Asaka, S. Eijima and H. Ishida, *On neutrinoless double beta decay in the  $\nu$ MSM*, *Phys. Lett.* **B762** (2016) 371–375, [[1606.06686](#)].
- [32] M. Drewes, B. Garbrecht, D. Gueter and J. Klaric, *Leptogenesis from Oscillations of Heavy Neutrinos with Large Mixing Angles*, *JHEP* **12** (2016) 150, [[1606.06690](#)].



- [33] P. Hernández, M. Kekic, J. López-Pavón, J. Racker and J. Salvado, *Testable Baryogenesis in Seesaw Models*, *JHEP* **08** (2016) 157, [[1606.06719](#)].
- [34] M. Drewes, B. Garbrecht, D. Gueter and J. Klaric, *Testing the low scale seesaw and leptogenesis*, *JHEP* **08** (2017) 018, [[1609.09069](#)].
- [35] T. Asaka, S. Eijima, H. Ishida, K. Minogawa and T. Yoshii, *Initial condition for baryogenesis via neutrino oscillation*, *Phys. Rev.* **D96** (2017) 083010, [[1704.02692](#)].
- [36] S. Eijima and M. Shaposhnikov, *Fermion number violating effects in low scale leptogenesis*, *Phys. Lett.* **B771** (2017) 288–296, [[1703.06085](#)].
- [37] J. Ghiglieri and M. Laine, *GeV-scale hot sterile neutrino oscillations: a derivation of evolution equations*, *JHEP* **05** (2017) 132, [[1703.06087](#)].
- [38] S. Eijima, M. Shaposhnikov and I. Timiryasov, *Freeze-out of baryon number in low-scale leptogenesis*, *JCAP* **1711** (2017) 030, [[1709.07834](#)].
- [39] S. Antusch, E. Cazzato, M. Drewes, O. Fischer, B. Garbrecht, D. Gueter et al., *Probing Leptogenesis at Future Colliders*, *JHEP* **09** (2018) 124, [[1710.03744](#)].
- [40] J. Ghiglieri and M. Laine, *GeV-scale hot sterile neutrino oscillations: a numerical solution*, *JHEP* **02** (2018) 078, [[1711.08469](#)].
- [41] BELLE collaboration, D. Liventsev et al., *Search for heavy neutrinos at Belle*, *Phys. Rev.* **D87** (2013) 071102, [[1301.1105](#)].
- [42] LHCb collaboration, R. Aaij et al., *Search for Majorana neutrinos in  $B^- \rightarrow \pi^+ \mu^- \mu^-$  decays*, *Phys. Rev. Lett.* **112** (2014) 131802, [[1401.5361](#)].
- [43] E949 collaboration, A. V. Artamonov et al., *Search for heavy neutrinos in  $K^+ \rightarrow \mu^+ \nu_H$  decays*, *Phys. Rev.* **D91** (2015) 052001, [[1411.3963](#)].
- [44] ATLAS collaboration, G. Aad et al., *Search for heavy Majorana neutrinos with the ATLAS detector in pp collisions at  $\sqrt{s} = 8$  TeV*, *JHEP* **07** (2015) 162, [[1506.06020](#)].
- [45] CMS collaboration, V. Khachatryan et al., *Search for heavy Majorana neutrinos in  $\mu^\pm \mu^\pm +$  jets events in proton-proton collisions at  $\sqrt{s} = 8$  TeV*, *Phys. Lett.* **B748** (2015) 144–166, [[1501.05566](#)].
- [46] CMS collaboration, A. M. Sirunyan et al., *Search for heavy neutral leptons in events with three charged leptons in proton-proton collisions at  $\sqrt{s} = 13$  TeV*, *Phys. Rev. Lett.* **120** (2018) 221801, [[1802.02965](#)].
- [47] I. Boiarska, K. Bondarenko, A. Boyarsky, S. Eijima, M. Ovchinnikov, O. Ruchayskiy et al., *Probing baryon asymmetry of the Universe at LHC and SHiP*, [1902.04535](#).
- [48] M. Drewes, J. Hajer, J. Klaric and G. Lanfranchi, *NA62 sensitivity to heavy neutral leptons in the low scale seesaw model*, *JHEP* **07** (2018) 105, [[1801.04207](#)].
- [49] S. Alekhin et al., *A facility to Search for Hidden Particles at the CERN SPS: the SHiP physics case*, *Rept. Prog. Phys.* **79** (2016) 124201, [[1504.04855](#)].
- [50] D. Curtin et al., *Long-Lived Particles at the Energy Frontier: The MATHUSLA Physics Case*, [1806.07396](#).
- [51] V. V. Gligorov, S. Knapen, M. Papucci and D. J. Robinson, *Searching for Long-lived Particles: A Compact Detector for Exotics at LHCb*, *Phys. Rev.* **D97** (2018) 015023, [[1708.09395](#)].

- [52] J. L. Feng, I. Galon, F. Kling and S. Trojanowski, *ForwArd Search ExpeRiment at the LHC*, *Phys. Rev.* **D97** (2018) 035001, [[1708.09389](#)].
- [53] F. Kling and S. Trojanowski, *Heavy Neutral Leptons at FASER*, *Phys. Rev.* **D97** (2018) 095016, [[1801.08947](#)].
- [54] D. Gorbunov and I. Timiryasov, *Testing  $\nu$ MSM with indirect searches*, *Phys. Lett.* **B745** (2015) 29–34, [[1412.7751](#)].
- [55] J. A. Casas and A. Ibarra, *Oscillating neutrinos and  $\mu \rightarrow e, \gamma$* , *Nucl. Phys.* **B618** (2001) 171–204, [[hep-ph/0103065](#)].
- [56] T. Asaka, S. Eijima and H. Ishida, *Mixing of Active and Sterile Neutrinos*, *JHEP* **04** (2011) 011, [[1101.1382](#)].
- [57] B. Pontecorvo, *Inverse beta processes and nonconservation of lepton charge*, *Sov. Phys. JETP* **7** (1958) 172–173.
- [58] Z. Maki, M. Nakagawa and S. Sakata, *Remarks on the unified model of elementary particles*, *Prog. Theor. Phys.* **28** (1962) 870–880.
- [59] I. Esteban, M. C. Gonzalez-Garcia, M. Maltoni, I. Martinez-Soler and T. Schwetz, *Updated fit to three neutrino mixing: exploring the accelerator-reactor complementarity*, *JHEP* **01** (2017) 087, [[1611.01514](#)].
- [60] A. Boyarsky, O. Ruchayskiy and M. Shaposhnikov, *The Role of sterile neutrinos in cosmology and astrophysics*, *Ann. Rev. Nucl. Part. Sci.* **59** (2009) 191–214, [[0901.0011](#)].
- [61] A. Abada, S. Davidson, A. Ibarra, F. X. Josse-Michaux, M. Losada and A. Riotto, *Flavour Matters in Leptogenesis*, *JHEP* **09** (2006) 010, [[hep-ph/0605281](#)].
- [62] O. Ruchayskiy and A. Ivashko, *Restrictions on the lifetime of sterile neutrinos from primordial nucleosynthesis*, *JCAP* **1210** (2012) 014, [[1202.2841](#)].
- [63] SHiP collaboration, M. Anelli et al., *A facility to Search for Hidden Particles (SHiP) at the CERN SPS*, [1504.04956](#).
- [64] PARTICLE DATA GROUP collaboration, C. Patrignani et al., *Review of Particle Physics*, *Chin. Phys.* **C40** (2016) 100001.
- [65] SHiP collaboration, C. Ahdida et al., *Sensitivity of the SHiP experiment to Heavy Neutral Leptons*, *JHEP* **04** (2019) 077, [[1811.00930](#)].
- [66] K. Bondarenko, A. Boyarsky, D. Gorbunov and O. Ruchayskiy, *Phenomenology of GeV-scale Heavy Neutral Leptons*, *JHEP* **11** (2018) 032, [[1805.08567](#)].
- [67] D. Gorbunov and M. Shaposhnikov, *How to find neutral leptons of the  $\nu$ MSM?*, *JHEP* **10** (2007) 015, [[0705.1729](#)].
- [68] “<https://doi.org/10.5281/zenodo.1407071>.”
- [69] J. Ghiglieri and M. Laine, *Precision study of GeV-scale resonant leptogenesis*, *JHEP* **02** (2019) 014, [[1811.01971](#)].
- [70] H. A. Weldon, *Effective Fermion Masses of Order  $gT$  in High Temperature Gauge Theories with Exact Chiral Invariance*, *Phys. Rev.* **D26** (1982) 2789.
- [71] M. Laine and M. Meyer, *Standard Model thermodynamics across the electroweak crossover*, *JCAP* **1507** (2015) 035, [[1503.04935](#)].

- [72] M. D’Onofrio and K. Rummukainen, *Standard model cross-over on the lattice*, *Phys. Rev.* **D93** (2016) 025003, [[1508.07161](#)].
- [73] I. Ghisoiu and M. Laine, *Right-handed neutrino production rate at  $T > 160$  GeV*, *JCAP* **1412** (2014) 032, [[1411.1765](#)].
- [74] D. Notzold and G. Raffelt, *Neutrino Dispersion at Finite Temperature and Density*, *Nucl. Phys.* **B307** (1988) 924–936.
- [75] J. Morales, C. Quimbay and F. Fonseca, *Fermionic dispersion relations at finite temperature and nonvanishing chemical potentials in the minimal standard model*, *Nucl. Phys.* **B560** (1999) 601–616, [[hep-ph/9906207](#)].
- [76] M. D’Onofrio, K. Rummukainen and A. Tranberg, *Sphaleron Rate in the Minimal Standard Model*, *Phys. Rev. Lett.* **113** (2014) 141602, [[1404.3565](#)].
- [77] “<http://www.laine.itp.unibe.ch/leptogenesis/>.”
- [78] M. Laine and Y. Schroder, *Quark mass thresholds in QCD thermodynamics*, *Phys. Rev.* **D73** (2006) 085009, [[hep-ph/0603048](#)].
- [79] S. Yu. Khlebnikov and M. E. Shaposhnikov, *Melting of the Higgs vacuum: Conserved numbers at high temperature*, *Phys. Lett.* **B387** (1996) 817–822, [[hep-ph/9607386](#)].
- [80] Y. Burnier, M. Laine and M. Shaposhnikov, *Baryon and lepton number violation rates across the electroweak crossover*, *JCAP* **0602** (2006) 007, [[hep-ph/0511246](#)].
- [81] S. Yu. Khlebnikov and M. E. Shaposhnikov, *The Statistical Theory of Anomalous Fermion Number Nonconservation*, *Nucl. Phys.* **B308** (1988) 885–912.
- [82] K. Radhakrishnan and A. C. Hindmarsh, *Description and use of lsode, the livermore solver for ordinary differential equations*, *Lawrence Livermore National Laboratory Report* (1993) .
- [83] E. Jones, T. Oliphant, P. Peterson et al., *SciPy: Open source scientific tools for Python*, 2001–.
- [84] “<http://www.netlib.org/odepack/>.”
- [85] W. R. Inc., “Mathematica, Version 11.3.”
- [86] T. Hambye and D. Teresi, *Baryogenesis from  $L$ -violating Higgs-doublet decay in the density-matrix formalism*, *Phys. Rev.* **D96** (2017) 015031, [[1705.00016](#)].
- [87] G. Sigl and G. Raffelt, *General kinetic description of relativistic mixed neutrinos*, *Nucl. Phys.* **B406** (1993) 423–451.
- [88] “Nufit 3.2 (2018), [www.nu-fit.org](http://www.nu-fit.org).”